UC Irvine

UC Irvine Electronic Theses and Dissertations

Title

Enhancing Atrial Fibrillation Detection Using Adaptive Template Matching

Permalink

https://escholarship.org/uc/item/3n82t2ww

Author

SUN, STEPHANIE

Publication Date

2023

Peer reviewed|Thesis/dissertation

UNIVERSITY OF CALIFORNIA,
IRVINE

Enhancing Atrial Fibrillation Detection Using Adaptive Template Matching

DISSERTATION

submitted in partial satisfaction of the requirements
for the degree of

DOCTOR OF PHILOSOPHY

in Electrical and Computer Engineering

by

Stephanie Sun

Dissertation Committee:
Professor Glenn Healey, Chair
Professor Anna Grosberg
Professor Rahim Esfandyarpour

2023

TABLE OF CONTENTS

LIST OF FIGURES

LIST OF TABLES

ACKNOWLEDGMENTS

VITA

Stephanie Sun

EDUCATION

Doctor of Philosophy in Electrical and Computer Engineering   **2023**
University of California, Irvine   *Irvine, California*

Master of Science in Integrated Technology Management   **2014**
California Polytechnic State University, San Luis Obispo   *San Luis Obispo, CA*

Bachelor of Science in Computer Science   **2013**
California Polytechnic State University, San Luis Obispo   *San Luis Obispo, CA*

RESEARCH EXPERIENCE

Graduate Research Assistant   **2014–2015**
University of California, Irvine   *Irvine, California*

TEACHING EXPERIENCE

Teaching Assistant   **2015**
University of California, Irvine   *Irvine, California*

REFEREED JOURNAL PUBLICATIONS

Enhancing Atrial Fibrillation Detection Using Adaptive Template Matching   **2023**
Under Review

REFEREED CONFERENCE PUBLICATIONS

Sun, Stephanie C., Xiaoyi Min, and Glenn Healey. "Investigation of Key Variables Impacting ICM Sensing Using Computer Simulations." *40th Annual International Conference of the IEEE Engineering in Medicine and Biology Society (EMBC)*. IEEE, 2018.

Sun, Stephanie C. and Glenn Healey. "Improving Atrial Fibrillation Detection Using Adaptive Template Matching (accepted)," *11th International Conference on Bioinformatics and Computational Biology (ICBCB 2023)*. 2023.

ABSTRACT OF THE DISSERTATION

Enhancing Atrial Fibrillation Detection Using Adaptive Template Matching

By

Stephanie Sun

Doctor of Philosophy in Electrical and Computer Engineering

University of California, Irvine, 2023

Professor Glenn Healey, Chair

Among all cardiac arrhythmia diseases, atrial fibrillation (AF) is the most prevalent and is associated with a chaotic and fast heartbeat, which often increases the risk of cardioembolic stroke and other heart-related problems, including myocardial infarction and progressive heart failure. Thus, it is important to diagnose AF in patients in the early stages and to have them receive proper treatment before the condition worsens. Surface electrocardiogram (ECG), implantable cardiac monitor (ICM), and Holter monitor analyses by doctors are the standard methods to diagnose AF in clinics. However, such analyses/diagnoses are time-consuming and sometimes difficult to interpret due to noise or data contamination. In this thesis, a new AF detection algorithm is proposed and evaluated using four available databases. Before discussing the new algorithms developed in this thesis, a basic introduction of the heart and its arrhythmia are reviewed in Chapter 1. An overview of existing AF detection methods and algorithms used in clinical and academic research is provided in Chapters 2 and 3. Chapter 4 is dedicated to exploring the real-life factors that impact AF detection. The new QRS template-based AF detection method is introduced and discussed in Chapter 5 through 7. It is shown that the new AF detection algorithm improves detection accuracy over standard methods in Chapter 8.

Chapter 1

Introduction

Arrhythmias are abnormal heart rhythms such as asystole and atrial fibrillation (AF). Clinicians diagnose and manage arrhythmias using electrocardiograms (ECGs) from devices such as Holter monitors, external loop recorders, post-event recorders, and insertable cardiac monitors (ICMs) [1] [2]. AF is the most frequently observed arrhythmia and is an irregular and often rapid heart rate that induces poor blood flow and can cause blood clots, stroke, and heart failure. This condition can be intermittent or continuous and sometimes causes symptoms such as fatigue, shortness of breath, dizziness, or palpitations [3]. In the United States, AF was the underlying cause of death for 26,535 people in 2019, and 12.1 million are projected to have AF in 2030 [4] [5] [6] [7].

A Holter monitor is a noninvasive technique for continuously recording ECGs for a few days using chest electrodes [1] [2]. An external loop recorder is the same as the Holter monitor but can continuously record ECGs for up to a month. A post-event recorder is placed directly on a patient's chest and records ECGs for up to a month like an external loop recorder. These devices allow a physician to identify arrhythmias without symptoms or to assess the overall arrhythmia burden over the recording period. However, the recording duration can

be insufficient if arrhythmic events are rare or vary over time. ICMs are implanted near a patient's heart and can monitor heart rhythms continuously for up to three years. They enable the detection of rare or varying events over time. ICMs also allow the continuous long-term monitoring of abnormal heart rhythms [8] and support the identification of symptom-rhythm correlations in patients with infrequent or unpredictable symptoms. In the case of AF, the ICM can be used for AF detection and to quantify the AF burden [9]. The long duration associated with ICMs increases the importance of developing automated processing techniques that can adapt to changes in the measured signals.

AF detection (AFD) with an ICM is commonly a rate-based algorithm that analyzes whether RR intervals are consistent or variable [10] [11] [12] [13] [14]. A critical challenge for these algorithms is the presence of ventricular ectopic beats which can lead to irregular RR intervals and false AF detection. This challenge has been addressed outside of the context of AFD using algorithms that analyze individual heartbeat morphological features, amplitudes, rhythm patterns, and correlations. Krasteva and Jekova [15] developed a method for identifying ventricular ectopic beats using a model derived from a set of three normal heartbeats selected by an operator. Decision rules based on signal descriptors are used to compare ECG waveforms to the model to recognize ectopic beats. Given a set of identified beats, de Chazal [16] used a set of time-domain features and a linear classifier to distinguish supraventricular and ventricular ectopic beats. Martinez, Alcaraz, and Rieta [17] used principal component analysis to model and remove ectopic beats from ECGs. This work only considered ectopic beats in ECGs containing AF, which may limit application to other signals.

In this dissertation, we develop automated methods for AF detection that use adaptive templates to differentiate normal and ectopic beats. Adaptive templates also estimate the number of P waves in an ECG segment. These templates are particularly useful for modeling changes in signal morphology due to factors such as measurement device position/orientation

2

change, which can occur during long-duration monitoring by devices such as ICMs. The methods utilize probabilistic models derived using logistic regression for the dependence of the likelihood of AF on various sets of measurable variables. We assess the methods using over 5000 ECG segments of 2.5 minutes from MIT-BIH databases. The assessment separately quantifies the benefit of the QRS and P wave templates for detection accuracy.

Chapter 2

Overview

2.1 Heart Rhythm Background

The human heart pumps blood through closed vessels to every tissue within the body [18] [19]. The blood delivers nutrients and oxygen to cells. When the cells and tissues do not receive blood, they stop functioning at their total capacity and can malfunction and die. The heart has four separate chambers: two atria (upper chambers) and two ventricles (lower chambers) (See Figure 2.1). A septum is a wall that separates the atria from the ventricles. The valves control blood flow within the four chambers. When blood becomes low in oxygen the heart pumps it to the lungs where oxygen is added for distribution across the body [19].

An electrical pulse initiates the heartbeat. The impulse starts in the sinoatrial (SA) node, which is a small bundle of specialized muscle cells located in the right atrium. The electrical activity travels through the atrial walls and stimulates contraction to force blood into the ventricles [20]. The SA node sets the heart's rate and rhythm. The impulse rhythmically repeats to drive the heartbeat and supply blood to the human body.
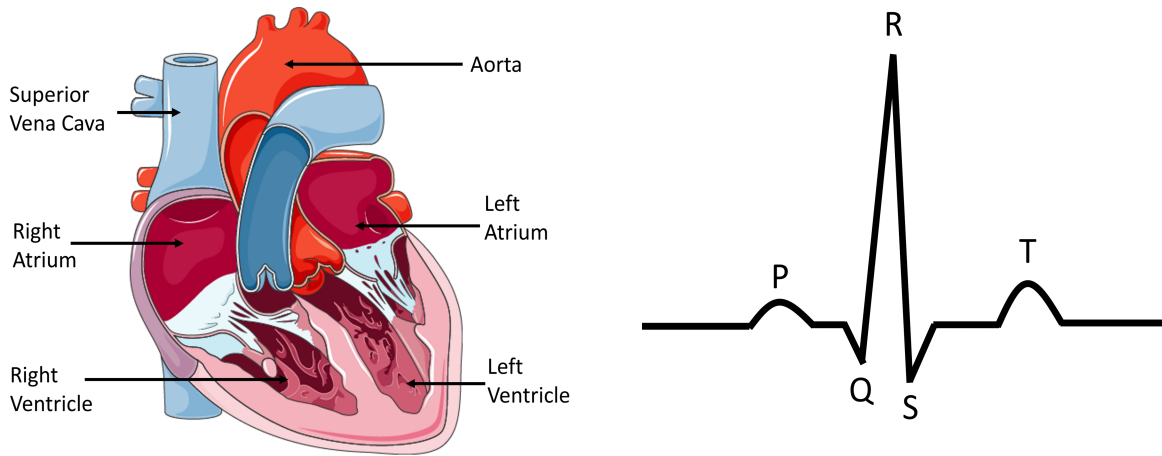
Figure 2.1: Typical heart anatomy and normal ECG rhythm waveform. Parts of the figure were drawn by using a picture titled "Heart" from Servier Medical Art. Servier Medical Art by Servier is licensed under a Creative Commons Attribution 3.0 Unported License (https://creativecommons.org/licenses/by/3.0/).

Cardiac arrhythmias are irregular heart rhythms, including tachycardia (very fast heart rhythm) and bradycardia (very slow heart rhythm) [21]. Some arrhythmia types are asymptomatic. When present, symptoms like palpitations, asystole (pause between heartbeats), lightheadedness, passing out, shortness of breath, or chest pain may occur in more serious cases [22]. While most arrhythmia cases are not serious, they can predispose a person to complications such as stroke, heart failure, and sudden death [23] [24].

Arrhythmias are often categorized into extra beats, supraventricular tachycardias, ventricular arrhythmias, and bradyarrhythmia [24] [25] [26]. Arrhythmias are due to the heart's electrical conduction system not working properly [23]. Several devices can help diagnose arrhythmias, including an electrocardiogram (ECG) and Holter monitor. In this chapter, we give an overview of typical arrhythmias for comparison to atrial fibrillation, which is most relevant to this dissertation topic.
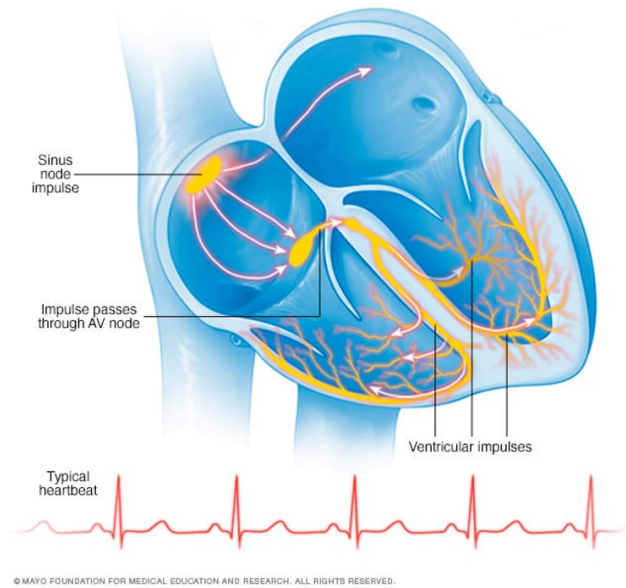
Figure 2.2: An illustration of typical heart rhythm

2.1.1   Normal Heart Rhythm

The SA node in the right atrium generates the heart rhythm by sending electrical signals that generally start each heartbeat [27]. The heart-signaling process usually goes smoothly in a healthy heart, resulting in a normal heart rate of 60 to 100 beats a minute (See Figure 2.1 and Figure 2.2) [27] [28] [29] [30]. However, an arrhythmia can occur if the heart beats too early, late, slowly, quickly, or at irregular intervals [3] [31] [32]. This arrhythmia happens because there is a dysfunction in the heart's electrical conduction system.

2.1.2   Atrial Fibrillation

Among the many different forms of arrhythmias, atrial fibrillation (AF) is the most common [3] [31] [32]. AF is an irregular and often very rapid heart rhythm. In other words, AF induces varying and often very fast or slow heartbeats. In AF, the electrical impulses in the atria (upper chambers of the heart) are disorganized and are unsynchronized or out of coordination with the ventricles (lower chambers of the heart). Examples of signals from a
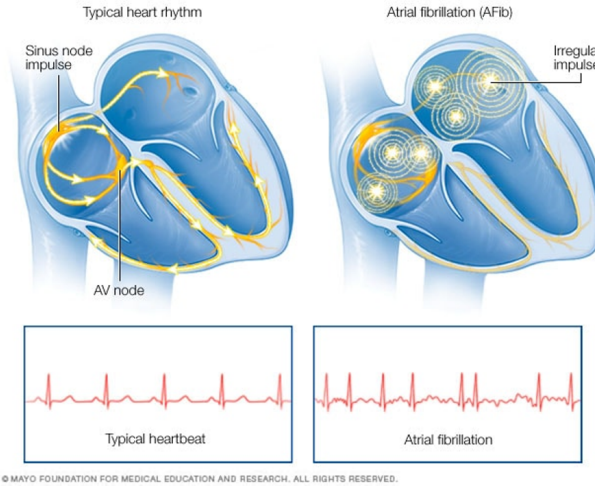
Figure 2.3: An illustration of atrial fibrillation

normal heart and with AF are seen in Figure 2.3 [3] [31]. It can be observed that the electrical impulses in the normal heart proceed in an orderly flow, but the electrical impulses in the AF heart are chaotic. In AF, the heart may pump over 150 times per minute due to irregular heart rhythm. But in a healthy heart, the heart pumps approximately 60 to 100 times per minute. During AF, the multiple ectopic foci in the atria discharge at an extremely fast rate which leads to multiple irregular stimulations. As the atria cannot respond mechanically to the disorganized electrical signal stimulation, the atria twitch rather than contract properly.

2.1.3 Atrial Flutter

In atrial flutter [33], the atria beat too quickly, as shown in Figure 2.4, causing a fast, but usually regular, rhythm. Atrial flutter is a type of arrhythmia caused by problems in the heart's electrical system. Atrial flutter is like AF, which causes abnormal heart beat patterns, but atrial flutter is more organized and less chaotic than AF. Sometimes a person may have both atrial flutter and AF. People with atrial flutter may be asymptomatic, but the disorder can increase the risk of complications such as stroke and heart failure.
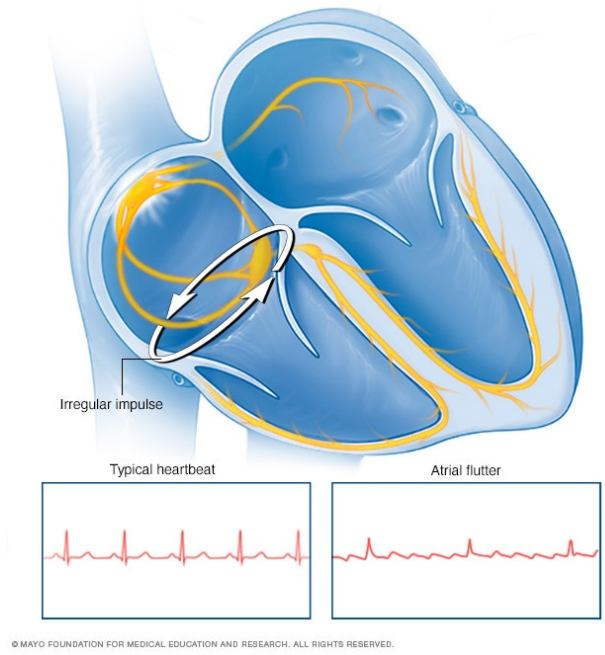
Figure 2.4: An illustration of atrial flutter

2.1.4 Supraventricular Tachycardia

Supraventricular tachycardia (SVT) is an abnormally fast or erratic abnormal heart rhythm that affects the atria (See Figure 2.5) [34]. SVT is also called paroxysmal supraventricular tachycardia. During an episode of SVT, the heart rate is about 150 to 220 times per minute, but it can occasionally beat faster or slower. Most people with SVT can have healthy lives without activity restrictions or treatment. Others may need to control or eliminate the rapid heartbeats and related symptoms.

2.1.5 Ventricular Tachycardia

Ventricular tachycardia (VT) is an arrhythmia due to irregular electrical signals in the ventricles (See Figure 2.6) [35]. A healthy heart typically beats about 60 to 100 times a minute at rest. In VT, the heart beats faster, usually 100 or more beats a minute. Sometimes the rapid heartbeat prevents the heart chambers from properly filling with blood. As a result,
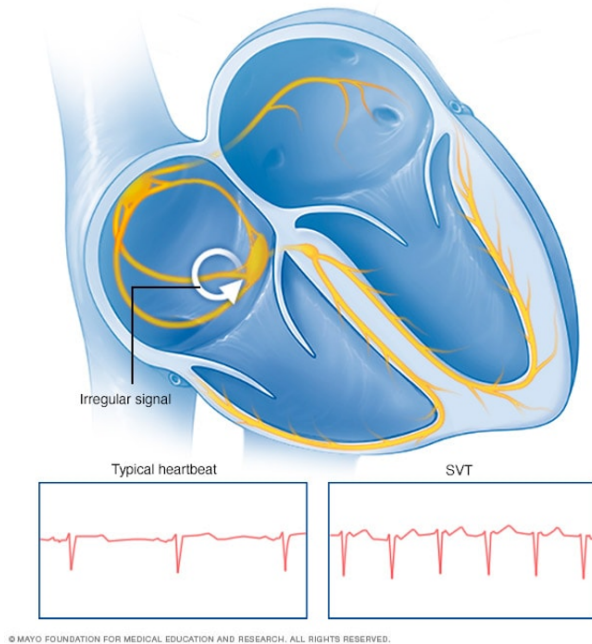
Figure 2.5: An illustration of supraventricular tachycardia

the heart may not be able to pump enough blood to the body. If this happens, a person may feel short of breath or lightheaded, or lose consciousness. VT episodes may be brief and last only a few seconds without harm. However, episodes more than a few seconds (sustained VT) can be life-threatening. Sometimes VT can cause sudden cardiac arrest.

2.1.6 Ventricular Fibrillation

Ventricular fibrillation (VF) is an arrhythmia [36]. During VF, disorganized heart signals cause the ventricles to twitch uselessly (see Figure 2.7). As a result, the heart doesn't pump blood to the rest of the body. Because VF is the most frequent cause of sudden cardiac death, it requires immediate medical attention.
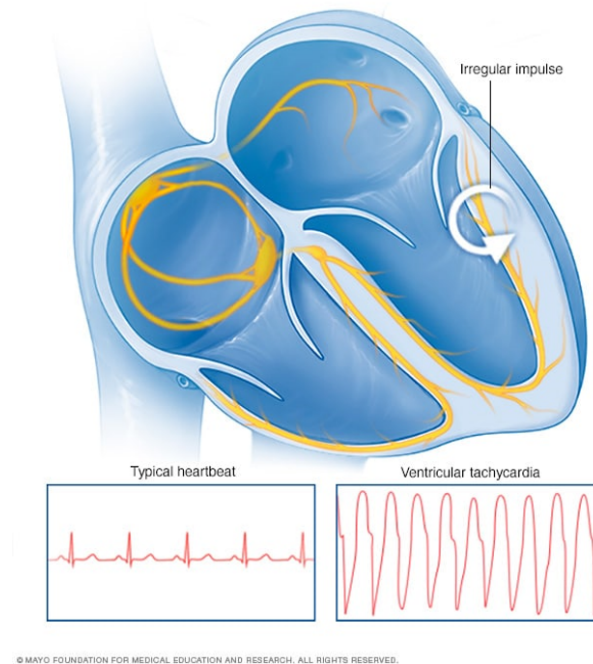
Figure 2.6: An illustration of ventricular tachycardia
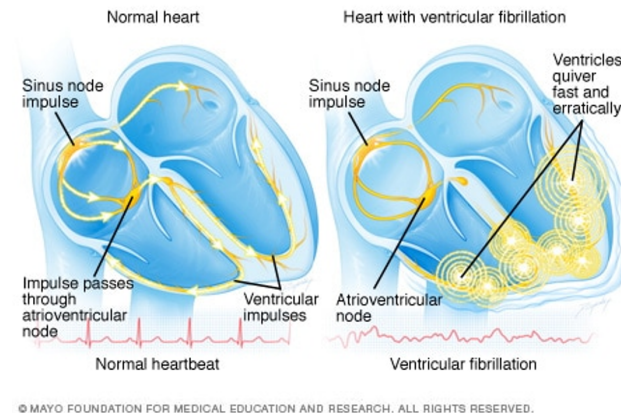
Figure 2.7: An illustration of ventricular fibrillation

2.1.7 Bradyarrhythmia

Bradyarrhythmia is a heart rhythm with a slow resting heart rate that is below 60 beats a minute that indicates the heart isn't pumping enough blood. Types of bradyarrhythmia include sick sinus syndrome (SSS), conduction block, and first-degree to third-degree atrioventricular (AV) blocks.

10

The SA node sets the heart's pace. If it doesn't work properly, the heart rate may alternate between bradycardia and tachycardia [37] [38]. SSS can be caused by scarring near the SA node that's slowing, disrupting, or blocking the travel of impulses. SSS is most common among older adults.

First-degree AV block is a disease in the heart's electrical conduction system in which electrical impulses conduct from the cardiac atria to the ventricles through the AV node more slowly than normal [39]. This block is generally asymptomatic, but it may become a second-degree and third-degree AV block. It is diagnosed using an ECG and is defined as a PR interval above 200 milliseconds. First-degree AV block affects 0.65-1.1% of the population, with 0.13 new cases per 1000 persons each year. When the heart's electrical pathways are blocked, it can cause the heartbeat stimulating signals to slow down or halt. Some blocks may lead to no signs or symptoms.

Second-degree AV block is a disease in the heart's electrical conduction system that blocks some of the atrial impulses to impair conduction between the atria and ventricles [40]. It is classified as an AV node block and is categorized between first-degree (slowed conduction) and third-degree blocks (complete block).

Third-degree AV block is a medical condition in which the nerve impulse generated in the SA node in the atrium of the heart cannot propagate to the ventricles [41]. Because the impulse is blocked, an accessory pacemaker in the lower chambers will typically activate the ventricles. This is known as an escape rhythm. Since this accessory pacemaker also activates independently of the impulse generated at the SA node, two independent rhythms can be noted on the ECG.
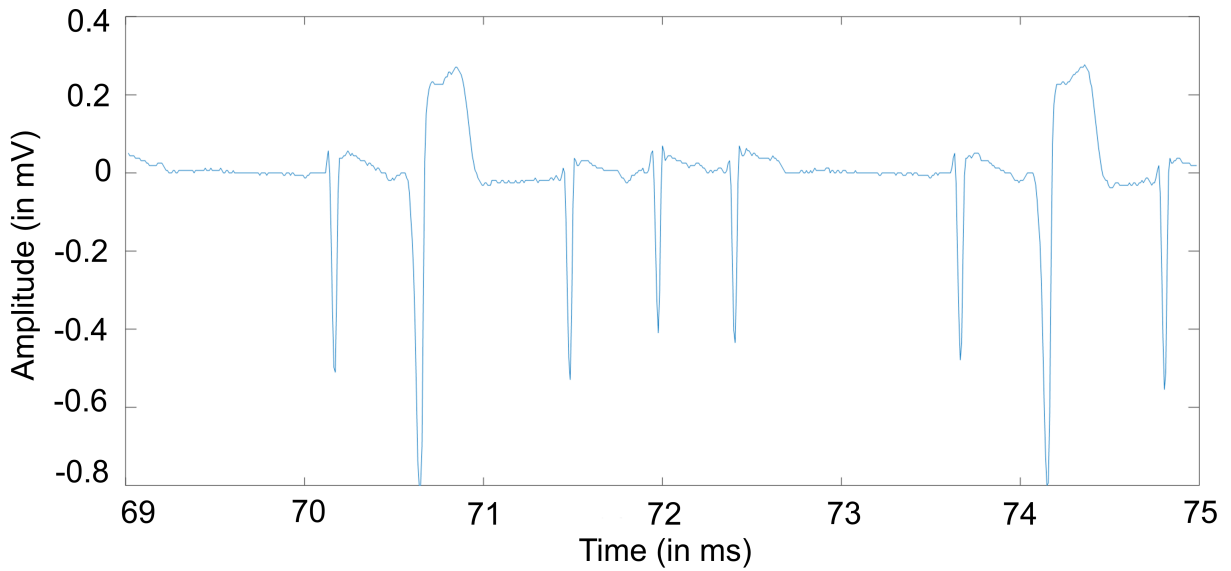
Figure 2.8: ECG of premature ventricular contraction episode. Premature ventricular contraction (PVC) is a beat with a morphology different from a sinus rhythm. QRS complexes of sinus rhythm are < 100 ms wide. QRS complexes of PVCs are broader (> 120 ms). PVCs occur earlier than expected on the next heartbeat, so their RR intervals as shown in this ECG are much shorter. PVCs can contribute to false appearances of RR irregularity, even though they have no P-waves.

2.1.8 Premature Heartbeats

Premature heartbeats are extra beats as seen in Figure 2.8, sometimes in patterns that alternate with the normal heartbeat. The extra beats may come from the atria (premature atrial contractions) or the ventricles (premature ventricular contractions). A premature heartbeat may feel like a skipped heartbeat. These beats are generally not concerning and rarely indicate a more severe condition. Still, a premature heartbeat can trigger a longer-lasting arrhythmia, especially in people with heart disease. Seldomly, persistent premature beats lasting several years may cause a weak heart. Premature heartbeats may occur when resting. Sometimes premature heartbeats are caused by stress, rigorous exercise, or stimulants like caffeine or nicotine.

2.2   ECG Monitoring Devices Background

2.2.1   Holter Monitor

A Holter Monitor is a familiar device to most practitioners and has been an effective choice for ECG monitoring [1]. It uses multiple ECG leads to efficiently record an arrhythmia's start, end, and length during the monitoring period [2]. However, most Holter Monitors can only store data for up to two days which is insufficient if symptoms are rarely repeated or if arrhythmic events vary extremely. Moreover, these devices lack real-time data analysis and incur considerable delay between ECG recording and analysis time. Newer devices, such as post-event and external loop recorders, address these drawbacks.

2.2.2   Post-Event Recorder

Unlike external loop recorders and Holter Monitors, post-event recorders are placed directly onto the chest area once a symptom appears [1] [2]. Although they can record ECGs for up to 1 month, they can store up to 5 to 6 minutes of continuous ECG data on patient activation. This happens at the onset of symptoms or after an abnormal episode. In that case, they do not continuously monitor for rhythms or denote the origin of arrhythmias. The start, end, and length of an arrhythmia episode may or may not be recorded. External loop recorders and insertable cardiac monitors address these drawbacks.

2.2.3   External Loop Recorder

External loop recorders look like Holter Monitors, but they can record for up to 1 month [1] [2]. They can store ECG segments of fixed length before and after activation either automatically by algorithms or manually through button presses. An external loop recorder usually

13

records 1 to 6 minutes of new ECGs, replaces previously recorded ECGs, and stores data only when activated either automatically or manually. The automated recorders can also detect some symptomless arrhythmias along with their start times. Although they obtain better symptom-rhythm correlations, they do not document cardiac activities continuously due to ECG storage limits. Insertable cardiac monitors eliminate this drawback.

2.2.4 Insertable Cardiac Monitor

An insertable cardiac monitor functions like an external loop recorder. Still, it is implanted near a patient's heart in the chest area and can monitor heart rhythms continuously for up to 3 years [1] [2]. Moreover, it provides additional documentation for analysis of cardiac activities compared to an external loop recorder, including data about rarely repeated symptoms and varying arrhythmic events. While close to the heart for better signal sensing, interpreting ECGs has several challenges: device orientation/position, device flipping, and respiration.

Chapter 3

AF Detection and Diagnosis

Atrial fibrillation (AF) causes severe health concerns that can result in mortality [42]. Computing devices and algorithms with the latest technological advancements can reduce AF-related risks by early detection and diagnosis [43]. In general, atrial fibrillation detection algorithms include rate-based AF detection [11] [13] [14] [44] [45], morphology-based detection [15] [16] [17] and machine learning and deep learning approaches [12] [46]. These algorithms help extract useful knowledge from data to aid decisions by doctors. Furthermore, different types of electrogram sensors can be used for identifying cardiovascular, gait, and other activities of daily life. In this chapter, we present an overview of state-of-the-art AF detection approaches that can be used for diagnosis and management. In summary, these detection algorithms are 1) Heart Rate-based algorithms, 2) Morphology-based algorithms, and 3) Automatic AI learning-assisted algorithms. These detection algorithms use data collected from a surface ECG or an implanted device such as an ICM.

3.1   AF Detection Challenges

AF detection using sensors outside the body can be challenging. For example, smartphone cameras obtain pulsatile signals from normal sinus rhythm (NSR) subjects but motion and noise artifacts corrupt those signals, causing the camera to detect them as AF [47]. Motion-corrupted episodes have a similar characteristic of irregular RR intervals to AF.

Several factors impact AF detection using ICMs. While an ICM is implanted close to the heart for better signal sensing, there are several challenges to interpreting ECGs [48]. R and P wave amplitudes vary greatly due to factors such as posture changes or motion, device orientation and position changes, respiration, noise, and body mass [48].

3.2   AF Detection Algorithm Efficacy

A few criteria can characterize AF detection algorithms' diagnosis performance. The most commonly used two parameters are sensitivity and specificity. A common method of presenting an algorithm's performance is the receiver operating characteristic [49].

3.2.1   Sensitivity

Sensitivity is a test's ability to detect patients with a condition such as a disease correctly. The sensitivity or detection rate in a clinical setting of a test is the proportion of those who test positive for the condition among those who truly have the condition. Mathematically, this can be expressed as:

$$\text{sensitivity} = \frac{\text{number\_of\_true\_positives}}{\text{number\_of\_true\_positives} + \text{number\_of\_false\_negatives}} \qquad (3.1)$$

A negative result in a high-sensitivity test is useful for ruling out the condition. The test is reliable when it shows a negative result since it rarely misdiagnoses those who have the condition. A test with 100% sensitivity indicates all patients with the condition test positive. However, a positive result in a high-sensitivity test does not always work for detecting the condition. Suppose a test kit is always designed to give a positive result. When used on patients with the condition, all patients test positive, leading to a test with 100% sensitivity. However, sensitivity does consider false positives. Moreover, this test will show positive on all healthy patients, rendering it useless for detecting or "ruling in" the condition.

3.2.2 Specificity

Specificity relates to a test's ability to determine that a patient does not have a condition. The specificity of a test is the proportion of those who test negative for the condition among those who truly do not have the condition. Mathematically, this can also be written as:

$$\text{specificity} = \frac{\text{number\_of\_true\_negatives}}{\text{number\_of\_true\_negatives} + \text{number\_of\_false\_positives}} \qquad (3.2)$$

A positive result in a high-specificity test is useful for ruling in the condition. The test rarely shows a positive result in any healthy patient. A positive result indicates a high probability of the presence of disease. A test with 100% specificity indicates all healthy patients test negative for the condition so that a positive test result would detect the presence of the

condition. However, a negative result in a high-specificity test does not necessarily work for ruling out the condition. For example, suppose a test always returns a negative test result to any patient. It gives a specificity of 100% because specificity does not include any false negatives. However, this test would show negative for all patients with the condition, making it useless for ruling out the condition.

3.2.3   Receiver Operating Characteristic Curve

The Receiver Operating Characteristic (ROC) curve can be used to compare the efficacy of AFD algorithms. It plots true positive and false positive rates to graphically display a binary classifier system's diagnostic performance at all of its discrimination thresholds. ROC analysis helps to evaluate the diagnostic tests' performance and, more generally, the accuracy of a statistical model that separates subjects into two categories (e.g., diseased or non-diseased).

3.3   Rate Based Detection Algorithm

3.3.1   Heart Rate Variability Based

AF detection can use heartbeat variability from inter-beat intervals [13]. The Poincare plot uses the inter-beat intervals to extract three feature measures - the number of clusters, mean step increment of inter-beat intervals, and point dispersion around a diagonal line in that plot - to characterize AF and non-AF [50]. AF is discriminated from non-AF using a support vector machine (SVM) with the mean stepping increment and point dispersion in the Poincare plot.

Since beats of ventricles are less likely to be influenced by baseline wandering and noise, the

use of inter-beat intervals to detect and diagnose AF can use a real-time portable monitoring electrocardiograph [50]. Such an algorithm requires only one lead of the ECG to acquire inter-beat intervals. Heart rate variability is closely related to the homeostasis of the autonomous nervous system. The dynamics of inter-beat intervals change after the onset of AF. People without AF show regular patterns in the Poincaré plots. However, the plots of AF patients are very irregular and change over time.

3.3.2   RR Interval Based

One AF detection algorithm is based on the characteristic of AF as a random sequence of heartbeat intervals with markedly increased beat-to-beat variability and complexity. This algorithm [10] combined three statistical techniques to exploit these characteristics, namely the Root Mean Square of Successive Differences (RMSSD) of RR intervals to quantify variability, the Turning Points Ratio (TPR) to test for randomness of the time series, and Shannon Entropy (SE) to characterize its complexity. In addition, in contrast to the Tateno–Glass method [10] [51] [52], which relies on training data histograms, this method is purely statistical and thus less dependent on the diversity of training data. Work in [10] considers AF to be random and employs a nonparametric statistic to test for randomness of the RR time series.

A rate-based algorithm is used in St. Jude Medical/Abbott devices [53]. AF and Non-AF R-R Interval Histograms capture the RR interval differences between AF rhythms and Non-AF rhythms. The histograms are templates for comparison with the histogram of an unknown ECG. On each heartbeat, the algorithm considers the last 64 beats to determine the three components: the probability of RR intervals irregularity, probability of random vs. patterned changes in RR intervals, and sudden onset score to detect if AF occurred.

3.4   Morphology Based Detection Algorithms

3.4.1   QRS Detection Algorithm

Another algorithm [54] employs QRS detection with integer arithmetic in real-time. A database with two simultaneous ECG channels is used. The algorithm uses a dual-threshold technique to find missed beats and reduce false negatives. There are two separate threshold levels where one level is half of the other. The thresholds continuously adapt to the characteristics of the signal since they are based upon the most-recent signal and noise peaks detected in the processed signals. If the algorithm does not find a QRS complex in a time interval equivalent to 166% of the current average RR interval, the maximal peak detected in that time interval that lies between these two thresholds is a possible QRS complex, and the lower of the two thresholds is applied. Unfortunately, the dual-threshold technique is only useful if the heart rate is regular.

Another approach [55] detects QRS complexes using slope, amplitude, and width information. A bandpass filter preprocesses the signal to reduce interference and allow high detection sensitivity with low amplitude thresholds. A dual-threshold technique is used to search for missed beats. The algorithm periodically adapts each threshold and RR interval limit automatically. This adaptive approach accurately uses ECG signals with diverse signal characteristics, QRS morphologies, and heart rate changes. However, this algorithm is limited when the sensitivity of episode detection cannot be ascertained because information about occurrences of under-detected AF is not available [56]. Thus, it was necessary to assume that the ECG at the onset represented the entire duration of the detected AF episode.

3.4.2   P Wave Detector

There is a need to improve the existing methods to achieve the highest efficiency possible [57]. RR intervals are straightforward to analyze, so AF detection algorithms assessing only heart rate are popular among today's ECG systems. In the presence of other significant RR fluctuations, e.g., ectopic beats or respiratory sinus arrhythmia, most methods produce significantly lower specificity. The method in [57] proposed an AF detection method based on a Poincaré plot of consecutive RR intervals [13], and it takes P waves into account as well to reduce the false positive cases in the presence of non-AF arrhythmias.

3.5   AF Detection from Surface ECG Recorder

An ECG is a non-invasive test that measures electrical signals produced by heartbeats. There are various types of ECG machines with different capacities for capturing data. For instance, a 12-lead 300 Hz ECG monitor can produce hundreds of millions of points for each patient [58]. The physicians analyze ECG data to identify heart diseases like AF, myocardial infarction, or acute hypotensive. Machine-learning and deep-learning approaches are employed to predict AF heart diseases.

A Holter Monitor is a portable ECG recording device that continuously records heart rhythms without requiring patient interactions with the device. It usually records for 24 to 48 hours (or longer in some newer devices). The data are stored on a flash drive that can be uploaded for analysis. The recorded data fully discloses arrhythmia from the entire recording period, which will help identify suspected frequently occurring silent arrhythmias or assess the overall arrhythmia burden. Like other external monitoring devices, there are scenarios in which Holter monitoring has not revealed a source of arrhythmia despite a high degree of suspicion. In other words, although certain arrhythmia is highly suspected, Holter

monitoring might not reveal its source.

The work in [59] has surveyed several methods and their merits and drawbacks. Some methods tend to employ too many ECG parameters to characterize AF, which results in increased computational complexity. To reduce the computational burden, methods have been attempted using fewer parameters for the characterization, which resulted in a trade-off in classification performance. The results on selected patients or segments were published in some cases, mainly due to the difficulty in parameter extraction.

3.6 AF Long Term Monitoring and Detection from Implanted Device

Insertable Cardiac Monitors (ICMs) are proven diagnostic tools to establish symptom rhythm correlation in cases where symptoms present infrequently, unpredictably, or in circumstances where an external monitor may be unfeasible [60] [61] [62] [63] [64] [65] [66]. They have the potential to alter both treatment and management plans for patients. Newer models of ICMs are smaller and, thus, easier to implant and explant. They also allow remote Bluetooth monitoring and may allow new specialized algorithms to better detect atrial fibrillation [60] [67].

Continuous monitoring is needed for patients with infrequent and unpredictable arrhythmia/symptoms. These arrhythmias would likely not be detected using conventional methods such as Holter monitoring that can only be used for a much shorter time. In the event of frequent (>2) false positive device-initiated transmissions, the device can be reprogrammed to enhance the specificity of the device-initiated transmissions during the patient's next in-person appointment.

3.7 AI and Machine-Learning for AF Detection

In general, for a machine-learning algorithm, there are three possible classifiers – (a) supervised, (b) unsupervised, and (c) reinforcement [31] [68].

(a) Supervised Learning: Supervised learning is possible when input training data and corresponding output variables exist. Hence, the algorithm can learn to map the input to the output via the training data.

(b) Unsupervised Learning: Unsupervised learning means only input data is available without corresponding output variables. Therefore, the model cannot be trained to map the input sample to the corresponding output. This type of learning draws inferences from the unlabeled dataset and finds hidden patterns to group the data accordingly.

(c) Reinforcement Learning: This learning self-trains continuously by trial and error. This type of learning is goal-oriented based on interacting with the environment.

(d) Deep Learning: Besides the first three learning processes, one can develop with deep learning techniques. A deep learning system is often composed of several artificial neural networks (ANN). The term 'deep' stems from the several hidden layers in the ANN structure. The primary building block of the ANN is the artificial neuron. The behavior and function of the artificial neurons are replicas of brain neurons [31] [69]. Deep learning is an established discipline, with algorithms conducted in many studies in diverse areas such as speech recognition [31] [70], handwriting recognition [31] [71], object detection [31] [72], and healthcare and medicine, including analysis of medical images [31] [73] and physiological signals [31] [74] [75] [76] [77] [78] [79].

The referred studies in [31] [75] [80] [81] suggest that the implementation of deep learning may improve the overall detection robustness as compared to the employment of conventional methods. Moreover, with deep learning, R-peak detection and the removal of noise and

artifacts from the ECG signals are not called for, and the extraction of features and the selection of hand-crafted features are unnecessary. However, the main pitfall of deep learning is the need for more training samples to train the networks for optimal performance.

3.7.1 Machine-Learning in AF Detection

Recent technological advancements in algorithms and computing devices can help reduce AF-related risks by detecting them in the early stages [58]. Deep learning and machine learning approaches extract helpful knowledge from historical training data to make application decisions. Furthermore, different types of developed sensors can be used to identify cardiovascular, gait, and other activities of daily life. These sophisticated sensors, computing devices, and intelligent algorithms provide opportunities to develop systems that can improve health and quality of life, such as detecting AF in the early stages.

AF can be a quiet stroke or asymptomatic AF, a rhythm that shows no symptoms. Unfortunately, detecting a quiet AF with such a short duration is difficult, even using a 12-lead electrocardiogram, because it requires longer monitoring intervals. The machine learning approaches can speed decision-making while improving AF diagnosis reliability, efficiency, and accuracy. Furthermore, machine learning can aid in developing a risk model to identify patients with a high risk of AF [58] [82].

The Support Vector Machine (SVM) is a supervised machine-learning algorithm that learns from examples with assigned labels. The range of applications of SVM includes disease classifying, natural language processing [58] [83], human activity recognition [58] [84], image processing [58] [85], fault detection, and diagnosis [58] [86] [87] [88] [89] [90].

The SVM is favored in scenarios where the volume of data is massive or the complexity of the data is very high [58] [91]. This technique can also be used for AF detection, where

complex test samples are obtained from patients suffering from the disease. The sample can be, for instance, a medical image compressed using the wavelet transformation. The SVM classifier can achieve excellent unbiased results in the training phase.

The widely used classifiers in detection systems include SVM and linear discriminant analysis for ECG arrhythmic detection. For more reliable and accurate AF detection, ANN takes the ECG signal's RR interval as input for classification. R peak is robust, and the ANN classifier is good at processing non-linear data. When trained and tested on the AF Termination Challenge Database and MIT-BIH Arrhythmia Database, this classifier gave a sensitivity of 99.3%, a specificity of 97.4%, and an accuracy of 98.3% [58].

3.7.2   Deep Learning Methods for AF Detection

Recently, the convolutional neural network (CNN) has gained much attention due to its performance in various applications such as image detection, time series analysis, and language processing. Time series analysis involves massive data used in many healthcare scenarios. CNN consists of fully interconnected convolutional layers comprised of neurons. A proposed CNN-based method in [58] [92] uses raw ECG signals. Another developed model uses a modified frequency slice wavelet transform (MFSWT) and CNN. The MFSWT performs better for low-frequency ECG signals, and its benefits include its precise time-frequency component position estimation and signal adaptiveness. MFSWT converts the ECG signal into 2D space, then images were given to 12-layered CNN, which extracts features of labeled images and calculates scores to sort the predicted image. For this system, the MIT-BIH AFDB database is used. This contains 25 ECG recordings collected from 25 subjects' data interpreted by a cardiologist. The time-lapse for each recording is 10 h and 15 min. Each ECG signal has 250 samples per second and its resolution is 12 bits in a range of 10 mV. The results from the above setup give an accuracy of up to 81.07% with five-fold cross-validation,

with sensitivity at 74.96% and specificity at 86.41%. CNN is a popular technique that combines extraction of features, reduction of features, and classification techniques. It classifies the data with a fully connected multilayer perceptron (MLP). The disadvantages of CNN include slow convergence speed and a lot of iterations.

Chapter 4

Simulation and Modeling of Key Variants Impacting AF Detection

4.1 Introduction

While many devices can record electrograms, an ICM is most frequently used for long-term monitoring and detecting AF episodes. An ICM is a small medical device placed under the chest muscle to continuously monitor electrical heart activities and record ECGs. Clinicians use ICMs to diagnose and manage abnormal heart activities, including those in patients with unexplained syncope, palpitations, cryptogenic stroke, lightheadedness, dizziness, and seizures. However, clinical studies [93] [94] [95] [96] [97] [98] have shown that false detection rates of abnormal heart rhythms are still high, and key variables can cause the ICM to detect heart signals inappropriately by altering the amplitudes and morphologies of ECGs.

In older ICM models, false diagnosis by oversensing fast beats and undersensing bradycardia is well-recognized [99]. Enhanced features in algorithms and device designs have greatly reduced inappropriate sensing. Clinical observations have shown that an ICM is 94.5%-97.3%

sensitive to true abnormal heart rhythm episodes and can positively predict 64%-74.8% of detected abnormal heart rhythm episodes [53] [100]. Some causes of false detections include undersensing of premature ventricular contractions (PVCs), undersensing of normal sinus rhythm before or after PVCs, small R-waves, sudden R-wave amplitude change, signal close to the threshold, and loss of electrode contact [96]. Key variables (e.g., respiration [97], device rotation/orientation, device position, device flipping, and body mass [98]) may be associated with causes of false detections. This chapter investigates the effects of these key variables on ICM sensing using computer simulations and a virtual human family.

4.2   Methods and Models Used

Sim4Life finite element analysis (FEA) software is used to simulate cardiac propagation and ICM electrode sensing inside three members of a virtual human family. The ICM CAD model was used and placed in each member at various locations and with electrodes facing up or down. The propagation vectors in the heart are approximated by fields created along the heart axis going in the direction from the left atrium (LA) and right atrium (RA) disc pair to the apex disc. After solving the models, the voltage difference on the electrodes is obtained for each simulation.

4.2.1   Sim4Life Virtual Human Family Body Models

A set of computable, high-fidelity 3D Virtual Population human anatomical models in Sim4Life was generated from magnetic resonance imaging scans of healthy patients [101]. Along with the tissue property database [102], the models fully represent global variations of human anatomy. Each model depicts a unique body type, with over 120 vital anatomical features and over 300 precisely identified tissues and organs. Simulations involving human

models access the database linking to tissues to produce accurate and comprehensive results [103]. Considering anatomical differences and body mass index (BMI) values, we used 3 models – obese male, male adult, and girl – in simulations (Table 4.1).

Table 4.1: General Information about Each Human Model

Model	Age[Years]	Height [m]	Weight [kg]	BMI [kg/m^2]
obese male	37	1.82	119.5	36.1
male adult	34	1.77	70.2	22.4
girl	11	1.49	34.0	15.3

4.2.2   ICM Device Model and Placement

The latest commercial ICMs are about the size of a AAA battery with devices from vendors such as Medtronic (1.2cc, Figure 4.1a) and Abbott (1.4cc, Figure 4.1b) with similar electrode designs on one side of the ICM. A similar solid model of an ICM was created and used in simulations (Figure 4.1c). The model ICM has an end electrode and a tip electrode on the front side with a spacing of 37.7 mm between them. The end electrode is shaped as a half circle with a diameter of < 7 mm and the tip electrode is close to a quadrilateral with a smaller area than the end electrode. According to clinical device positions, this device was placed beneath the chest muscle of each of the three selected family members (Figure 4.2a). In each member, the device was modeled near the fifth rib at five positions to test position sensitivity (Figure 4.2b). The positions are labeled as DF_V = vertical position (clinical position), DF_45 = 45-degree rotation (clinical position), DF_H = horizontal position, MV3cm = vertical orientation shifted 3 cm to member's left side, and MH3cm = horizontal orientation shifted 3 cm up. In addition, the device is flipped for all five positions. The device is denoted as "face up" or "face down" when the electrodes face the skin or the heart, respectively.

(a) Medtronic ICM

(b) Abbott ICM

(c) The model: blue is the end electrode and red is the tip electrode

Figure 4.1: ICM model compared to Medtronic and St. Jude Medical ICMs
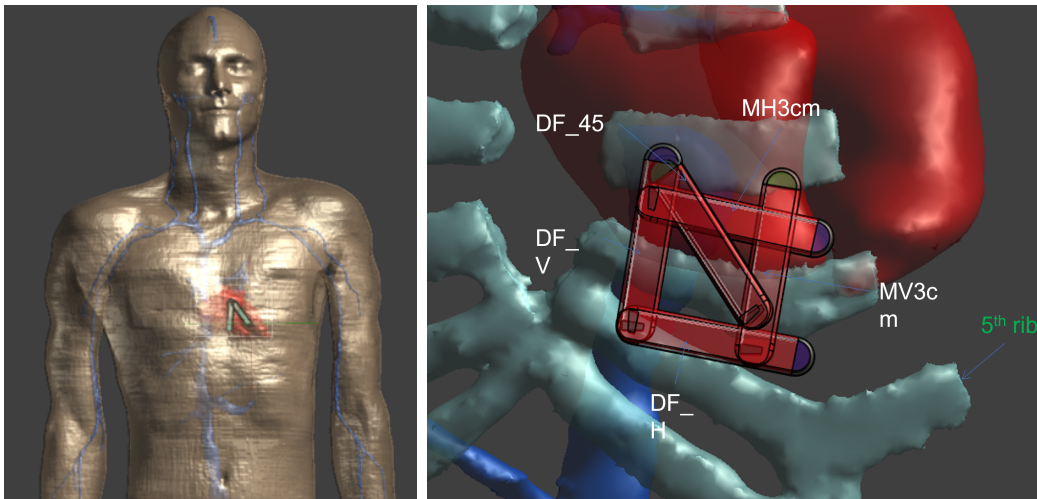
(a) Clinical device positions in adult male

(b) Device placement near the fifth rib at five positions

Figure 4.2: Device placement for simulation
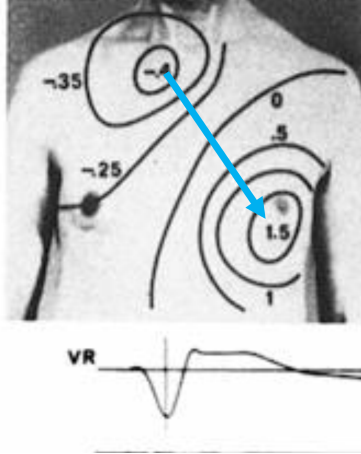
Figure 4.3: Electrical potential distribution of potential body map on a patient with cardiac vector along the heart axis pointing from local minimum to local maximum.

4.2.3 RA, LA, and Apex Disc Models

Three circular discs were modeled for each selected family member to mimic cardiac ventricular propagation. Two of the discs were fit inside the RA and LA above the valves, whereas the third disc was scaled according to the size of the apex and placed close to it. This forms the cardiac vector along the heart axis (Figure 4.3). The voltage difference between the atrium disc pairs and the apex disc is 1 V. The discs generated an electrical potential with a similar potential distribution on the body surface to that generated by cardiac ventricular propagation in sinus rhythm, so they were used to simulate sensed voltages on ICM devices. Evidence of the electrical potential distribution generated by cardiac ventricular propagation is explained in a previous study on patient-specific ECG models [104] [105] [106].

4.2.4 Sim4Life Electro Static Simulation Setup

Sim4Life electrostatic solvers were used in simulations to calculate the sensed voltages on the ICM electrodes inside the family members. The ICM header and box were set as dielectric materials, whereas the electrodes were set as perfect electrical conductors (PECs). In each electrostatic solver, the electrical conductivity of the lungs was either 0.046 S/m or 0.1 S/m

for simulating inflated or deflated lungs, respectively. Neumann and Dirichlet boundary conditions were used in the electrostatic solvers. The Neumann boundary condition was applied on six planes enclosing the body surface, whereas the Dirichlet boundary conditions were applied to the discs. The RA and LA discs were set to 0 V constant potential, and the apex disc was set to 1 V constant potential to obtain the voltage difference of 1 V between them. Field sensors record electrical fields in the electrostatic solvers. The overall field sensor records the human model's electric field and electric potential. The electric field is calculated as a negative gradient of electrical potential. The boxes surrounding each family member's heart muscle and discs were also set as field sensors. The line between two ICM electrodes on the same side of the ICM was set as a voltage sensor for recording the voltage between them. This sensed voltage is the input to the sensing circuitry of the ICM electrodes.

4.2.5 Normalization of Voltages

The average R-wave amplitude of 600 uV for normal body weight was divided by the extracted voltage from the simulation with the male adult model and the device at position DF_45 to obtain the scaling factor [98]. This scaling factor was then multiplied into an extracted voltage for each simulation to normalize it to clinical data.

4.3 Simulation Results

4.3.1 Electrical Potential Distributions

The electrical potential distribution body surfaces in all three members are similar, and 45 degrees tends to give greater potential drops at appropriate positions along the vectors (Figure 4.4). The patterns of the distributions are like those measured in humans at the

(a) Male Adult   (b) Obese Male   (c) Girl
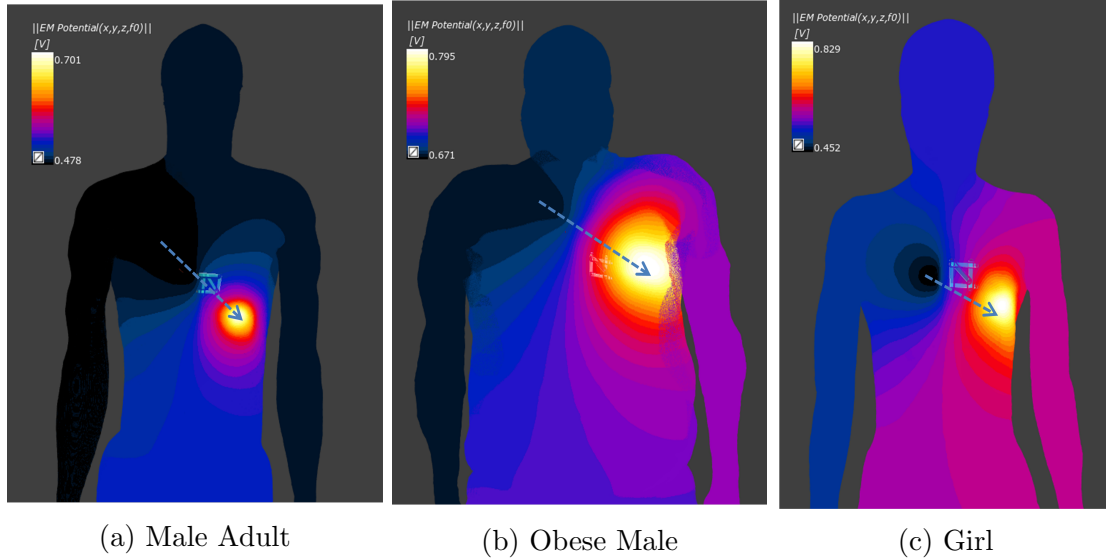
Figure 4.4: Electrical potential distributions on body surfaces of three models

peaks of QRS complexes [104] [105].

4.3.2 Sensing Voltage in Three Human Models

Voltages (V) are extracted from voltage sensors of ICM electrodes in each family member for device flipping, device orientation and migration, and respiration (Table 4.2).

Male Adult

Device Flipping: At device positions DF_45 and MV3cm, the sensed voltage had the smallest difference of 0.30% and the second smallest difference of 1.20%, respectively, with device flipping. At other device positions (DF_H, MH3cm, and DF_V) the differences were 2.05%, 5.38%, and 10.73%, respectively.

Device Positions or Rotation: When facing up, the sensed voltage had the average V= 522.82 $\pm$ 125.42 μV at all five device positions, with the maximum at DF_H (643.91 μV) and the minimum at DF_V (346.74 μV), that led to the most change by 46.15% between DF_H and

Table 4.2: Normalized voltages sensed by device along vector formed by discs with 1 V difference with each combination of key variables

Position	Rotation	Flipping	Respiration	Obese Male Mag ΔV (μV)	Male Adult Mag ΔV (μV)	Girl Mag ΔV (μV)
DF_45	45	Face Down	Deflate	295.29	600.00	1018.07
DF_45	45	Face Up	Deflate	281.42	601.80	1001.22
DF_V	0	Face Down	Deflate	13.59	309.52	254.83
DF_V	0	Face Up	Deflate	8.11	346.74	359.14
DF_H	90	Face Down	Deflate	400.08	630.71	1601.68
DF_H	90	Face Up	Deflate	390.12	643.91	1404.61
MV3cm	0	Face Down	Deflate	33.05	591.14	608.91
MV3cm	0	Face Up	Deflate	31.43	584.06	425.86
MH3cm	90	Face Down	Deflate	516.32	414.05	1049.29
MH3cm	90	Face Up	Deflate	494.43	437.58	995.99
DF_45	45	Face Down	Inflate	294.24	685.80	981.26
DF_45	45	Face Up	Inflate	285.97	632.42	954.20

DF_V. When facing down, the sensed voltage had the average V = 509.09 ± 140.22 μV at all five device positions. The sensed magnitude decreased the most by 50.92% when the device moved between DF_H (630.71 μV) and DF_V (309.52 μV). A greater maximum change for the device face down was observed than for the face up.

Respiration: When the lungs inflated, the magnitude increased by 12.51% and 4.84% for device face down and face up, respectively.

Obese Male

Device Flipping: At device position DF_H, the device had the smallest difference in sensed magnitude of 2.49% with device flipping. At other device positions (MH3cm, DF_45, MV3cm, and DF_V), the differences were 4.24%, 4.69%, 4.89%, and 40.32%, respectively.

Device Positions or Rotation: When facing up, the sensed voltage had the average V = 241.11 ± 215.79 uV at all five device positions. The sensed magnitude decreased the most

by 98.36% when the device moved between MH3cm (494.43 μV) and DF_V (8.11 μV). When facing down, the sensed voltage was V = 251.67 $\pm$ 222.73 μV at all five device positions. The sensed magnitude decreased the most by 97.37% when the device moved between MH3cm (516.32 μV) and DF_V (13.59μV).

Respiration: When the lungs inflated, the magnitude decreased by 0.35% and increased by 1.59% for the device face down and face up, respectively.

Girl

Device Flipping: At device position DF_45, the device had the smallest V difference of 1.65% with device flipping. At other device positions (MH3cm, DF_H, DF_V, and MV3cm), the differences were 5.08%, 12.30%, 29.05%, and 30.06%, respectively.

Device Positions or Rotation: When facing up, the sensed voltage had the average V = 837.37 $\pm$ 439.26 μV at all five device positions. The sensed magnitude decreased the most by 74.43% when the device moved between DF_H (1404.61 μV) and DF_V (359.14 μV). When facing down, the sensed voltage had an average 906.56 $\pm$ 507.28 μV at all five device positions. The sensed magnitude decreased the most by 84.09% when the device moved between DF_H (1601.68 μV) and DF_V (254.83 μV).

Respiration: When the lungs inflated, the sensed magnitude decreased by 3.62% and 4.70% for device face down and face up, respectively.

4.3.3 Body Mass

At the clinical default device position of DF_45, the simulated sensed magnitude decreased by at least 50.8% when changing between the adult male and the obese male. This is similar

to clinical data [98] with a mean decrease of 41.6% when BMI increased from an adult male to an obese male. When BMI decreased from the male adult to that of the girl, the simulated sensed magnitude increased by at least 66.4% while the clinical mean increased by 58.3% [98].

4.4 Discussion

Using RA, LA, and apex discs creates electrical sources for modeling large dipoles during ventricular depolarization, generating an electrical potential distribution on the body surface similar to that of the measured electrical potential for a human at the QRS peak in a sinus rhythm [106]. Instead of using a full propagation model that is computationally expensive [104] [105], the close relationship to the measured body potential supports a simplified approach. The absolute values of simulated body potentials can be calibrated with those measured in a human. If sensing of atrial propagation or PVCs needs to be simulated, a different selection of excitation vectors can be used.

A larger body mass is commonly associated with a longer distance between the heart and the electrodes in the subcutaneous layers of the body so that electrical sources inside the heart are farther away from the sensing electrodes. Therefore, smaller signals are typically sensed. The simulation results clearly show that a larger body mass generates smaller sensed signals among the three models simulated. These simulation trends are consistent with clinical observations in 281 patients [98] that increased body mass index was associated with lower measured R wave amplitude. Patients with a BMI > 35 had sensed R-waves near the minimum suggested amplitude by the device manufacturers of 300 μV. Simulations in the obese model had a maximum sensed R-wave amplitude of about 300 μV, which became lower as the ICM position changed.

Additionally, in the obese male model, much smaller signals were sensed, and the sensed

magnitude of signals changed greatly when the device position changed or flipped. The electric potential distributions on body surfaces in these three human models (Figure 4.4) also showed that sensed amplitudes could be highly sensitive to the device's orientation and position. The simulation results support that the largest changes (40% -98%) were when the device was changed from horizontal to vertical positions. The potential map also indicates that the recommended clinical 45 degrees would not necessarily guarantee the best R-wave sensing, and it depends on the location relative to the potential body map. This means that an external testing tool may be helpful.

It has been observed that the devices in patients could flip. The simulations in this study show that at the clinically recommended device position DF_45, the difference during device flipping was small in all three models (0.30%-4.69%). But the amount of change can be significant with the vertical orientation of the device (10%-40%), depending on position.

Respiration was simulated by changing the conductivity of the lung for inflated and deflated values but did not consider the changes in lung volume and corresponding device positions associated with respiration. The simulated respiration effect was small, likely due to the small amount of lung tissue between the device and the heart.

Chapter 5

AF Detection Algorithm Design

Figure 2.1 plots the ECG for a typical heartbeat, which includes a P wave, a QRS complex, and a T wave. AF is characterized by irregular intervals between R locations and the absence of P waves. For example, Figure 5.1 plots the ECGs for typical AF episodes with irregular RR intervals. AF detection (AFD) with an ICM is typically based solely on whether the RR intervals are consistent or variable [10] [11] [12] [13] [14]. These algorithms, however, can have false positive detections due to rhythms with variable RR intervals such as sinus arrhythmia, irregular sinus tachycardia, supraventricular tachycardia, and frequent premature ventricular contraction (PVC) that are not AF [15] [16] [17] [99] [107]. ECG examples of these rhythms are shown in Figure 2.8 and Figure 5.2 to Figure 5.5. These false positives can be avoided by detecting the presence of P waves. P-wave detection, however, can be challenging due to factors such as PVCs, Ventricular Flutter, and Ventricular Fibrillation [17]. In addition, P-wave detection is often complicated by variations in P-wave structure due to factors such as respiration, noise, body mass, or changes in device orientation and position [10] [48]. Examples of P-wave variation are shown in Figure 5.5 to Figure 5.8. We develop an algorithm for AFD that is robust to these factors by combining adaptive templates for QRS complexes and P waves with a measure of RR interval consistency.
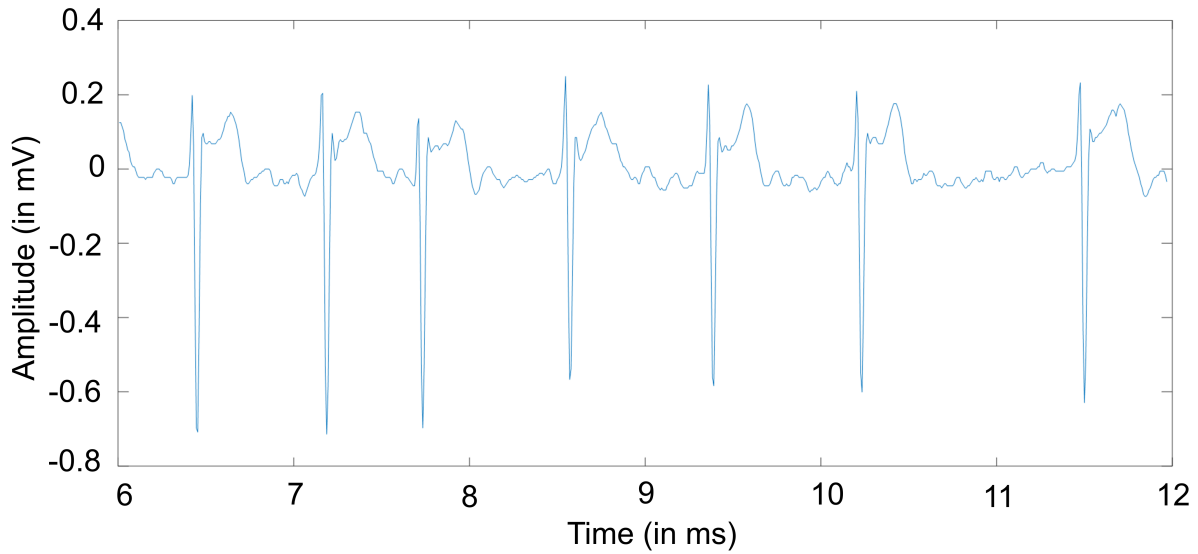
Figure 5.1: ECG of atrial fibrillation episode with irregular and often rapid heart rate that induces poor blood flow. The AF episode has irregular RR intervals with no P waves.
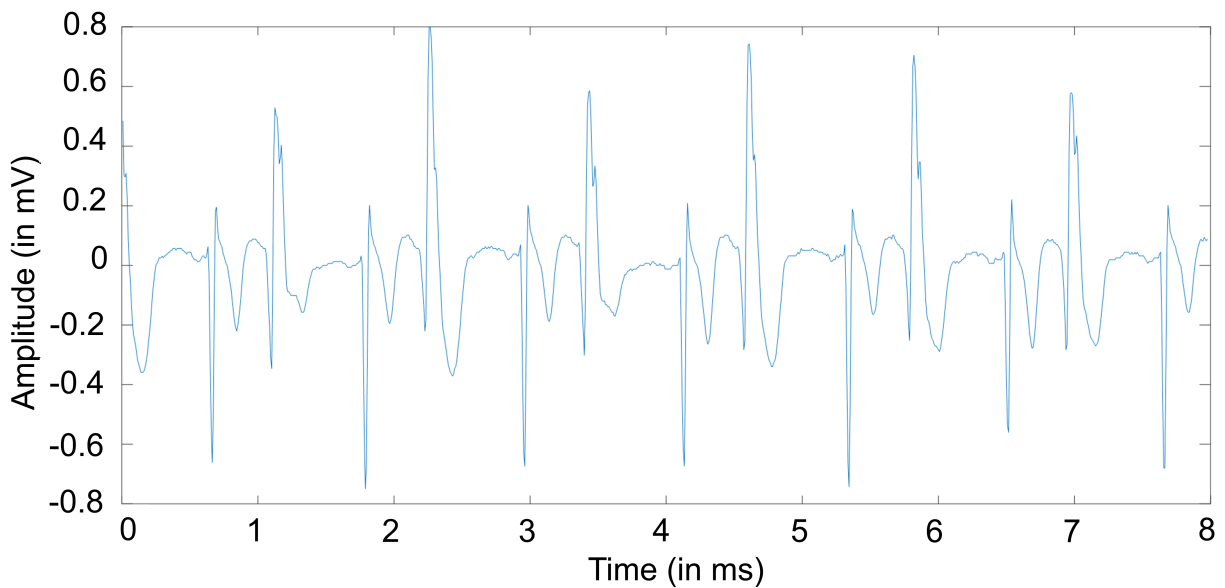
Figure 5.2: ECG of bigeminy with a QRS complex with alternating sinus rhythm and premature ventricular contraction causing RR intervals of different lengths.

The AFD Algorithm processes ECG segments using four modules: R wave detection, irregular rate detection, QRS Template Matching, and P Wave Detection. Each of these modules computes descriptors of the ECG segment that contribute to AF detection. The R wave

39
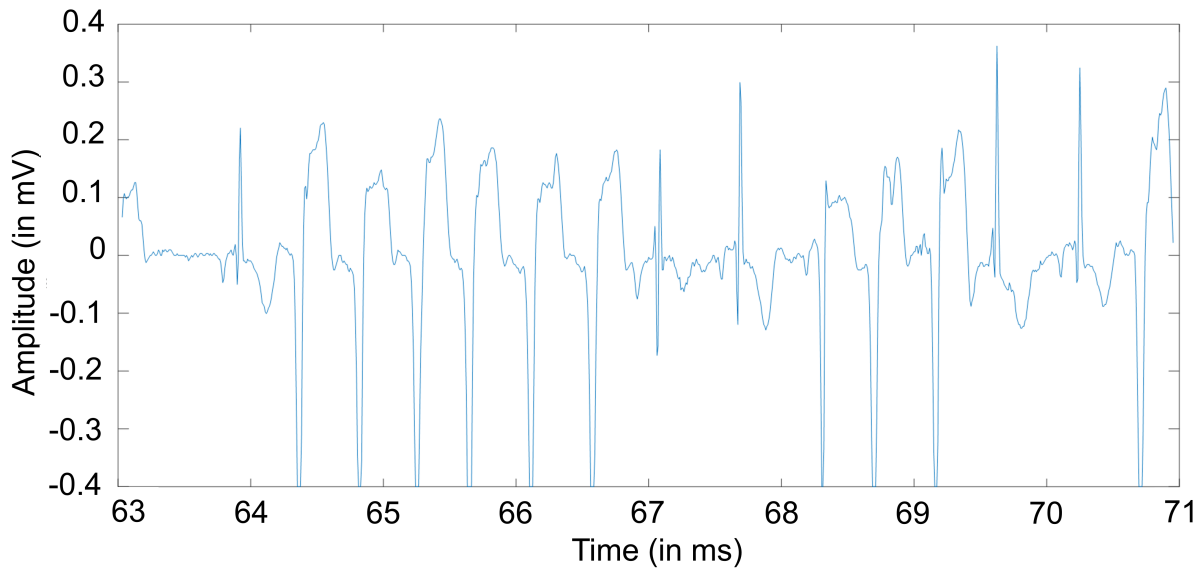
Figure 5.3: ECG of ventricular tachycardia episode with unique and broad (>160ms) QRS complexes which are different from those of a sinus rhythm.
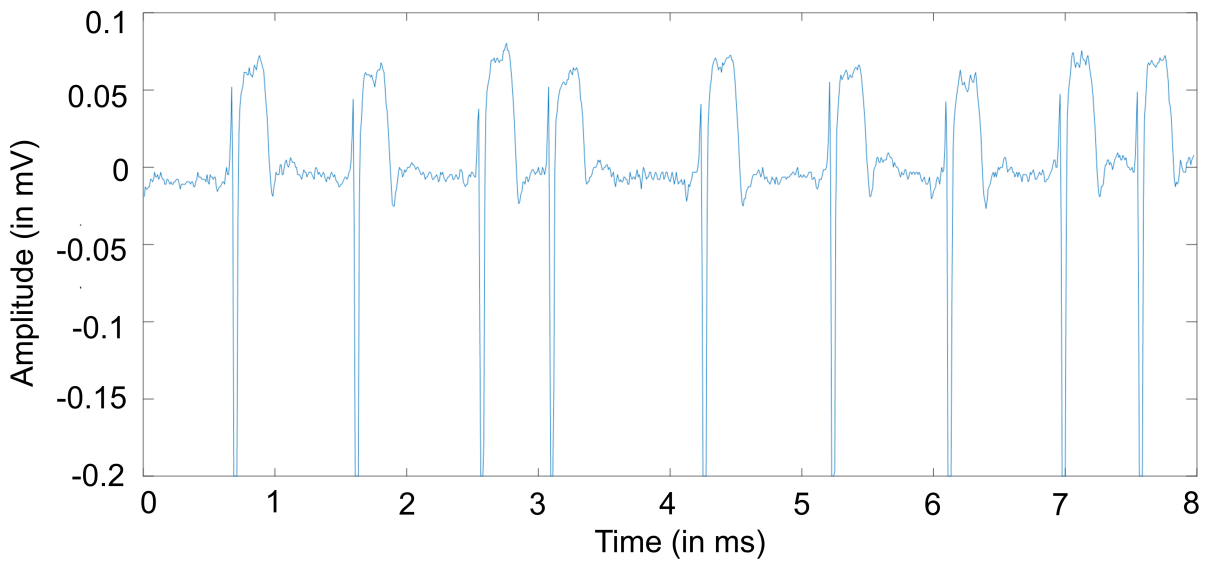
Figure 5.4: ECG of premature atrial contraction (PAC) episode with a morphology that is different from the one from a sinus rhythm. PACs can occur earlier than expected for the next heartbeat, or they can occur without any accompanying QRS complexes.

detector estimates the total number of R waves in the segment. The irregular rate detector computes a measure of the RR interval consistency. The QRS template matching process generates and updates templates that are used to refine estimates of the number of R waves
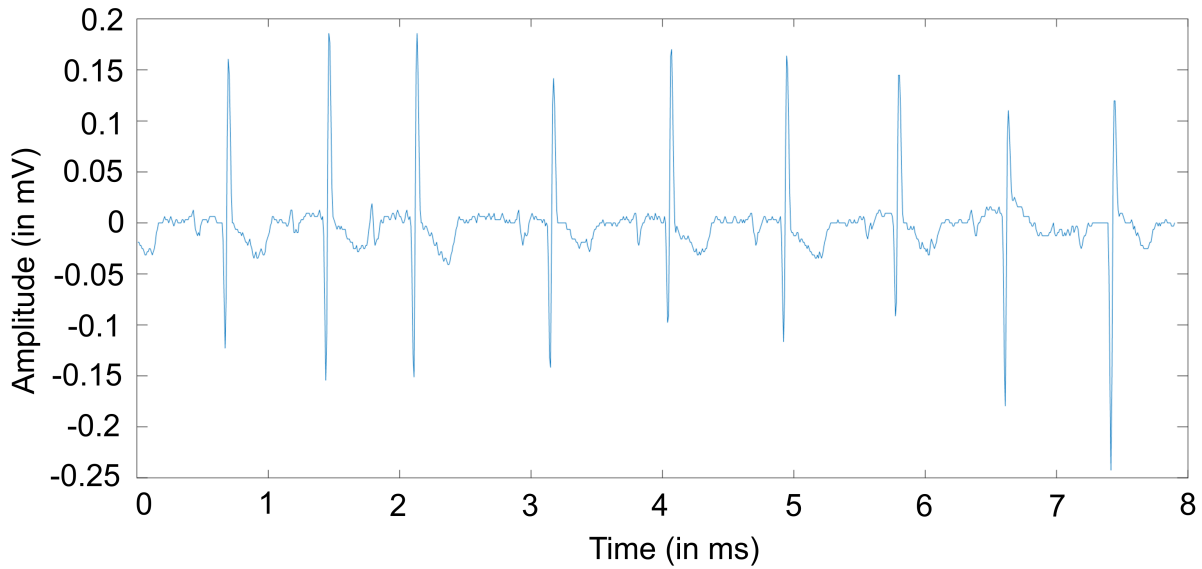
Figure 5.5: ECG of sinus arrhythmia with irregular RR intervals and with P waves with variable structure due to noise.
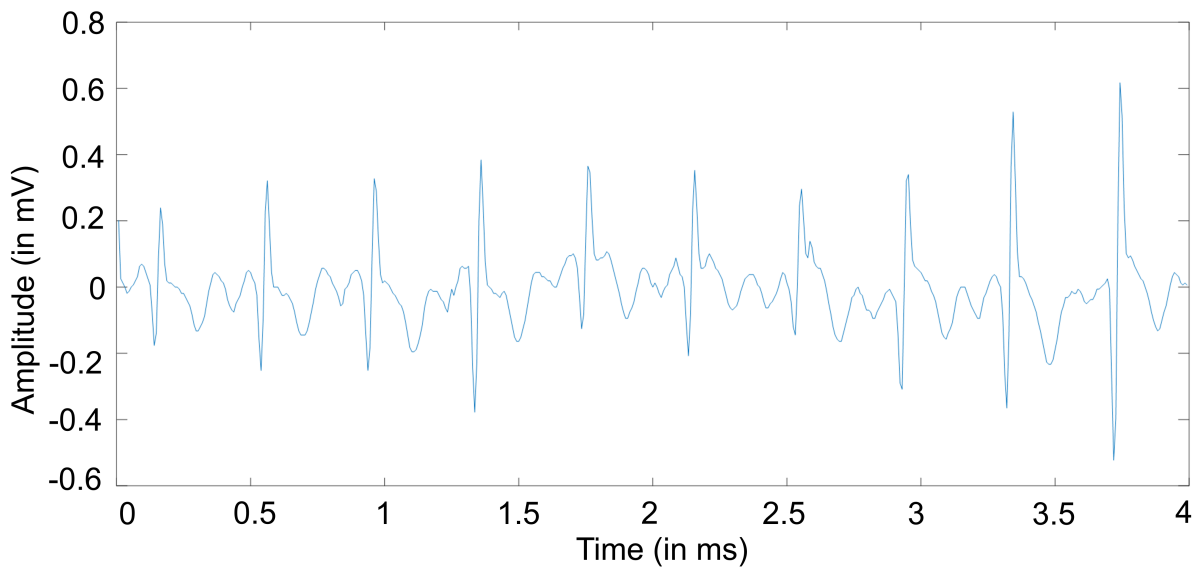
Figure 5.6: ECG of sinus tachycardia with a heart rate of > 150 bpm and inconsistent P waves. Sinus tachycardia can be mistaken for AF because it has no P-waves and irregular RR intervals.

and the consistency of the RR intervals based on QRS complexes that match the current template. The P Wave detector estimates the number of P waves in the segment. The descriptors generated by the modules are used to build a probabilistic model for the likelihood

41
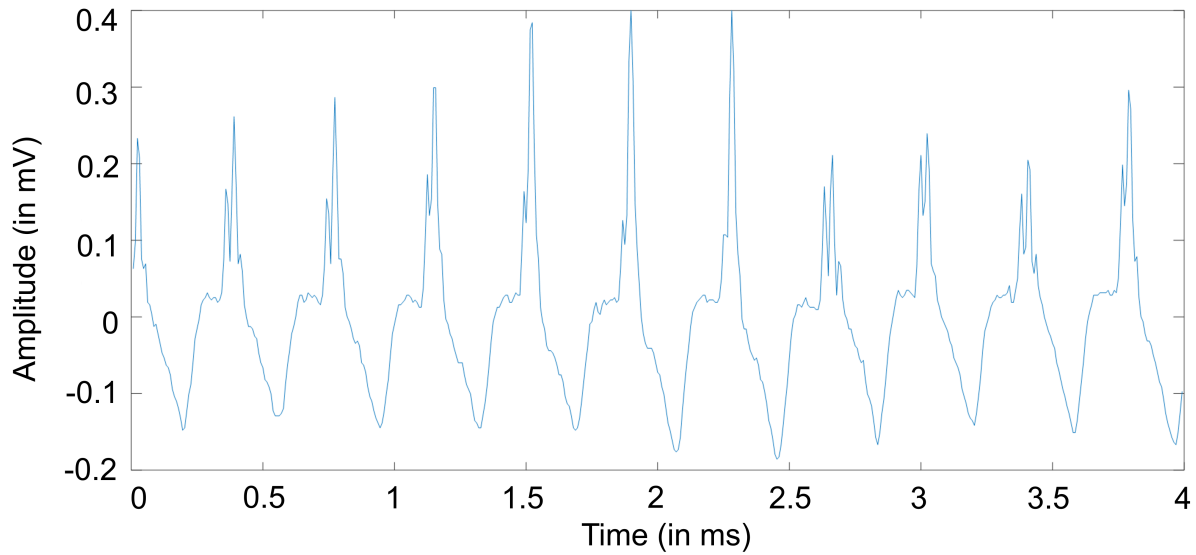
Figure 5.7: ECG of atrial tachycardia with abnormal P wave morphology due to origin from the upper heart chambers.
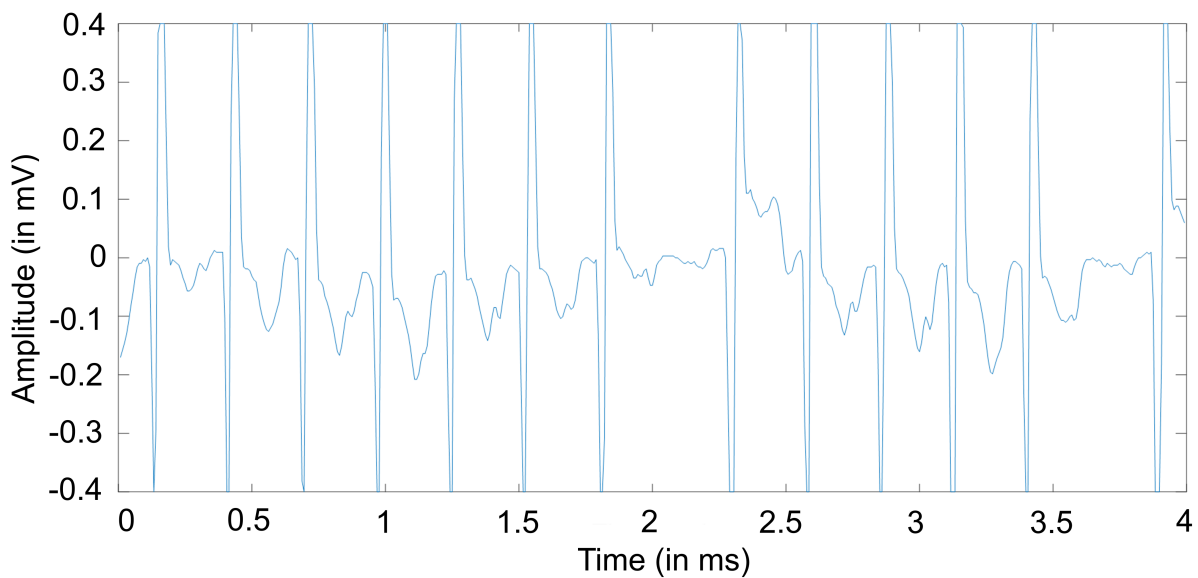
Figure 5.8: ECG of supraventricular tachycardia episode with narrow (< 120ms) QRS complexes and variable P waves due to overlap with T waves.

of AF using logistic regression. Figure 5.9 summarizes the components of the AF detection algorithm.
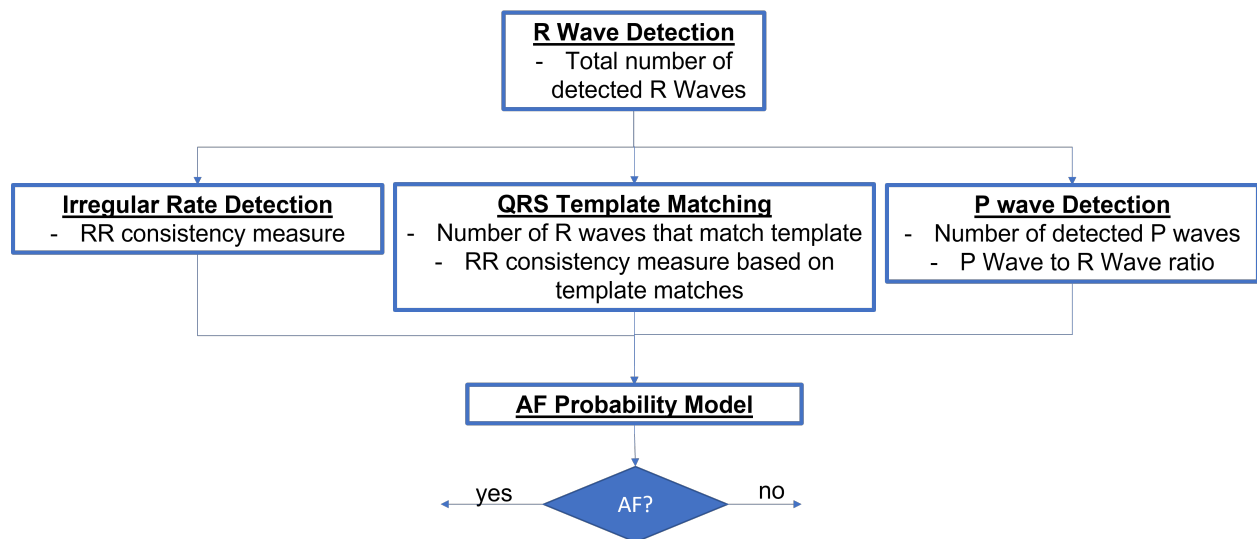
Figure 5.9: Components of AF detection algorithm

Chapter 6

R Wave Detection and Interval Consistency

The first step in the AFD algorithm is to detect R waves and to compute a measure of the consistency of the RR intervals. A threshold is used to locate the R waves in an ECG segment (See Figure 6.1), and we define $a(i)$ to be the sequence of positive time differences between successive R waves. If $n+1$ R waves are detected then there will be n RR intervals represented in $a(i)$. We define the RR consistency measure C [59] [108] using the coefficient of variation (CoV) of RR intervals.

$$C = \left\lfloor \frac{\sigma(|a|)}{\mu(|a|)} * 100\% \right\rfloor \tag{6.1}$$

where $\mu(|a|)$ is the mean of the absolute value of all elements in the sequence a and $\sigma(|a|)$ is the standard deviation of the absolute value of all elements in the sequence a. C will take a minimum value of zero if all of the RR intervals in $a(i)$ are the same and will increase
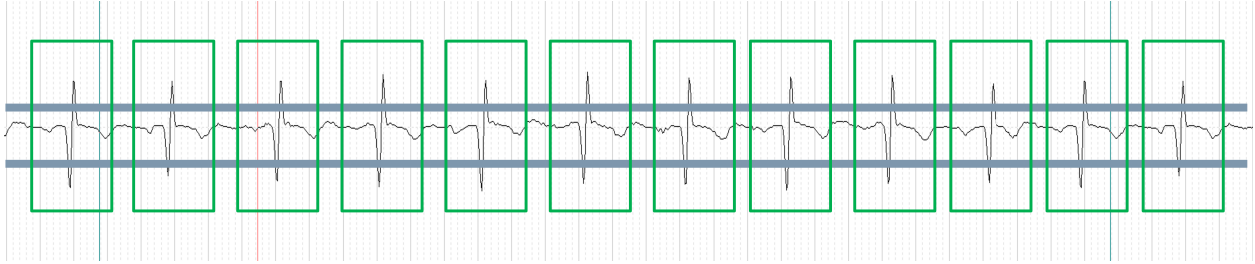
Figure 6.1: Detection of R waves with one of two thresholds
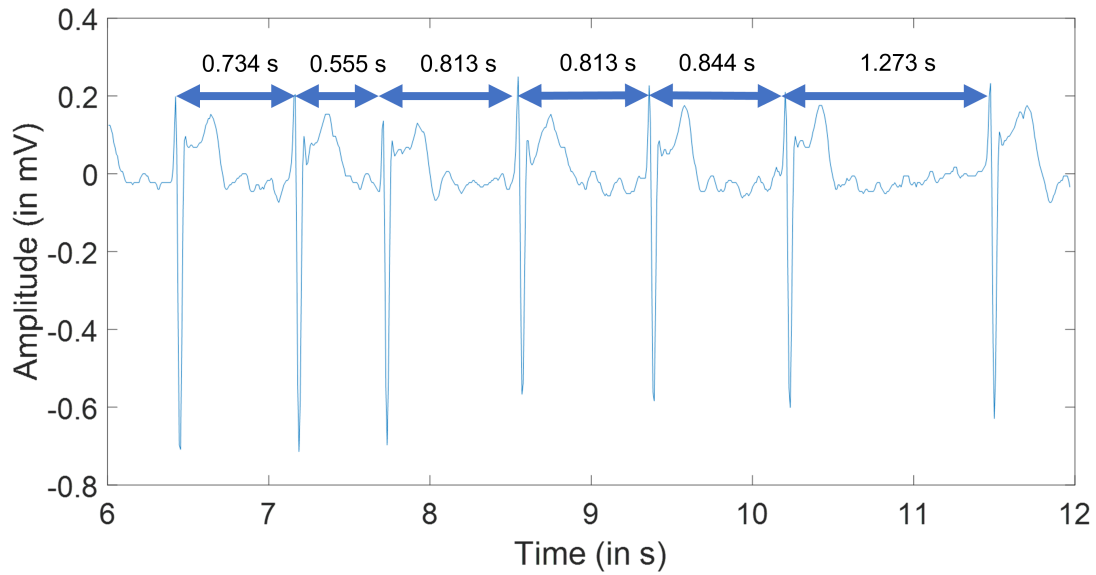
Figure 6.2: ECG of AF episode where the arrows indicate irregular RR intervals with their lengths in seconds

as successive RR intervals exhibit more variability. For the example in Figure 6.2 we have $\mu(|a|) = 0.839s, \sigma(|a|) = 0.343s$, and $C = 40\%$. The result of C indicates that the RR intervals vary significantly. The AFD algorithm calculates C for each ECG segment.

Chapter 7

Template Matching

7.1 Existing Ventricular Ectopic Beat Detection Algorithms

Existing ventricular ectopic beat detection algorithms analyze heartbeat morphological features, amplitudes, rhythm patterns, and correlations to reduce the false detection of sinus rhythms [15] [16] [17]. A principal component analysis-based algorithm detects QRS complexes based on the Phasor Transform [17]. The algorithm characterizes the QRS morphology of a beat with five descriptors: amplitude of R-wave peak, area of QRS complex, number of samples between γ_{iQRS+} and γ_{iQRS-}, number of samples between ρ_{iQRS+} and ρ_{iQRS-}, and the absolute value of the local minimum amplitude. γ_{iQRS+} and γ_{iQRS-} are the two closest points to the R-wave peak in which the amplitude falls to at most 30% of the peak amplitude. ρ_{iQRS+} and ρ_{iQRS-} are the two closest points to the local minimum in which the amplitude magnitude is at most 30% of this minimum amplitude magnitude.

A QRS template matching algorithm [15] selects up to three original templates (the most

frequently seen supraventricular or paced complexes) and substitutes their copies continuously throughout the ECG analysis to capture slight variations in heartbeat morphology of a patient's rhythm. The algorithm is based on three descriptors: area differences, frequency spectrum differences, and maximal cross-correlation coefficient.

A single-lead ECG-based algorithm is also used to detect supraventricular beats [16]. It uses 4 feature groups: RR intervals, heart-beat intervals, segmented morphology, and fixed interval morphology. They are organized into two feature sets. The first set contains RR intervals, heart-beat intervals, and segmented morphology. The second set contains RR intervals and fixed interval morphology. After processing these feature sets for each beat, the algorithm runs a linear discriminant classifier over them.

The approach in [17] is evaluated over individual beats of simulated and real AF signals. This algorithm is focused on AF only whereas our approach focuses on both AF and not AF signals. The method developed in this thesis also takes into consideration the full shape of the QRS complex for template matching. Our approach is not limited by linear discriminant nor does it track the number of samples compared to the algorithms in [16] [17].

7.2 Template Generation

QRS templates for a patient can be used to distinguish normal from ectopic beats. Let $E[n]$ be a discrete-time ECG signal and let t_i be the index of the central time sample for the ith QRS complex that is detected in the signal using a threshold as described in Chapter 6. Each complex is represented using $2W + 1$ time samples. The area under the curve of the ith complex is given by
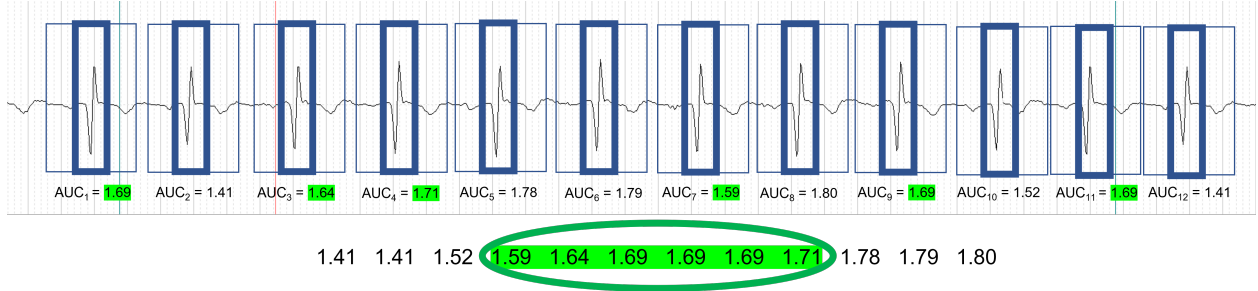
Figure 7.1: ECG segment with selected QRS complexes

$$A(i) = \sum_{n=t_i-W}^{t_i+W} |E[n]|. \tag{7.1}$$

After $A(i)$ is computed for the first N QRS complexes, the complexes that correspond to the interquartile range of $A(i)$ values are selected as model complexes. For our work we use N=12 to select 6 QRS complexes. Fig. 7.1 plots an ECG segment with 6 of 12 QRS complexes selected using the interquartile range of $A(i)$.

Let $x_j[n]$ for $0 \leq n \leq 2W$ be the signal for the jth selected QRS complex. Each of these signals is aligned to $x_1[n]$ by finding the value of the shift k denoted k_j that maximizes the cross-correlation

$$R[k] = \sum_{n=-\infty}^{\infty} x_j[n]x_1[n-k] \tag{7.2}$$

where each $x_j[n]$ is assumed to have value zero outside of the range $0 \leq n \leq 2W$. Figure 7.2a shows two QRS complexes before alignment by k_j and Figure 7.2b shows these complexes after alignment. Figure 7.3 shows a set of six selected complexes after alignment. A template $T[n]$ for $0 \leq n \leq 2W$ is generated by averaging the aligned selected complexes at each time

(a) Before alignment of complexes   (b) After alignment of complexes
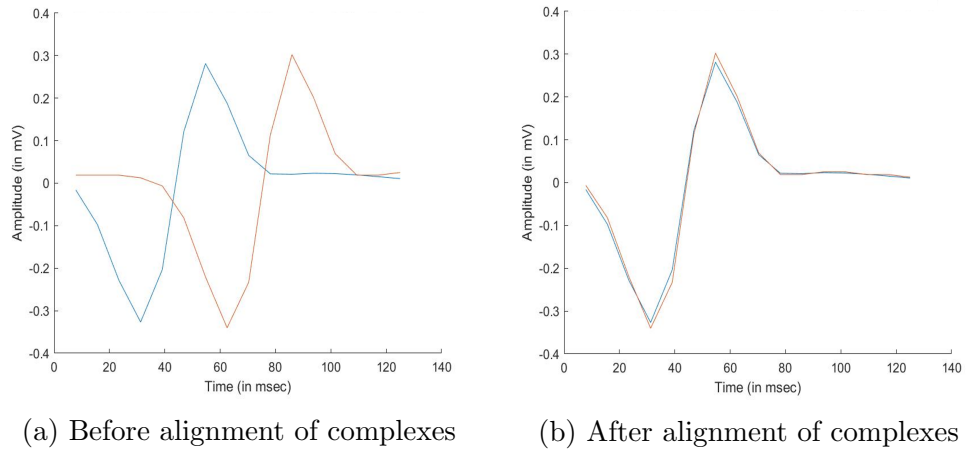
Figure 7.2: Example of alignment for 2 QRS complexes
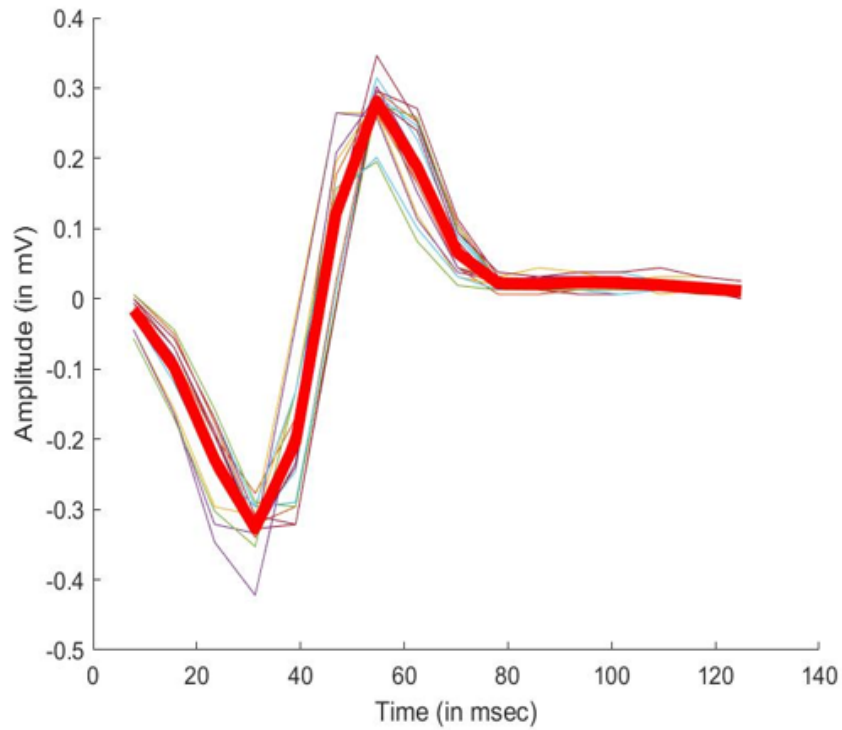
Figure 7.3: QRS template in red constructed by averaging selected complexes

sample as illustrated by the red curve in Fig. 7.3.

7.3 Template Matching and Update

The template $T[n]$ is used to identify subsequent abnormal beats in the ECG segment. Let $y_i[n]$ $(i = 1, 2, \ldots)$ for $0 \le n \le 2W$ be the signals for detected QRS complexes in the segment after alignment to the current template $T[n]$ using cross-correlation. Starting with $i = N + 1$ each detected complex $y_i[n]$ is compared with the current template $T[n]$ using the RMS difference measure

$$D(y_i, T) = \sqrt{\frac{\sum_{n=0}^{2W} (y_i[n] - T[n])^2}{2W + 1}}. \tag{7.3}$$

If $D(y_i, T)$ is less than a threshold then $y_i[n]$ matches the template $T[n]$. Figure 7.4 illustrates the comparison between a template and a series of QRS complexes.

The QRS template can be updated if the amplitude and morphology of the beats change over time. If N consecutive $y_i[n]$ complexes do not match the current template $T[n]$, then an updated template is generated by applying the process described in Section 7.2 to the N complexes. This updated template is compared with subsequent QRS complexes $y_i[n]$ using the difference measure in equation (7.3). We give an example of a template update in Figure 7.5. The current template at the beginning of the sequence is shown in red with each of the first ten QRS complexes. This template matches the first two complexes and then fails to match each of the next eight as shown by the green checks and red x's above the ECG. A new template is derived from beats three to ten and applied starting with beat eleven, circled in yellow. Starting with beat eleven, nine of the next twelve complexes match the updated template. Figure 7.6 shows more detailed comparisons between a template and a beat before and after update from Figure 7.5. The original template is for a sinus rhythm (SR) and is updated to a template for ventricular tachycardia (VT) which is a series of
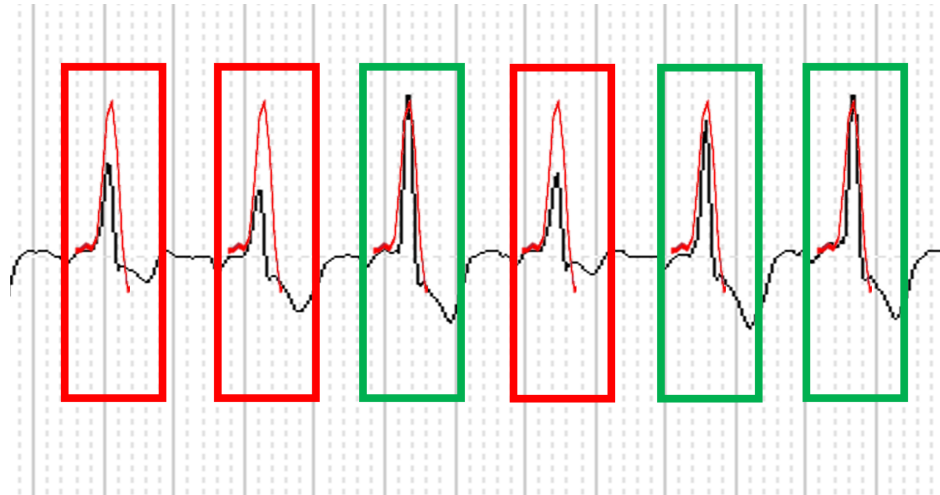
Figure 7.4: ECG example of QRS template matching. The 3rd, 5th, and 6th complexes match the template shown in red.
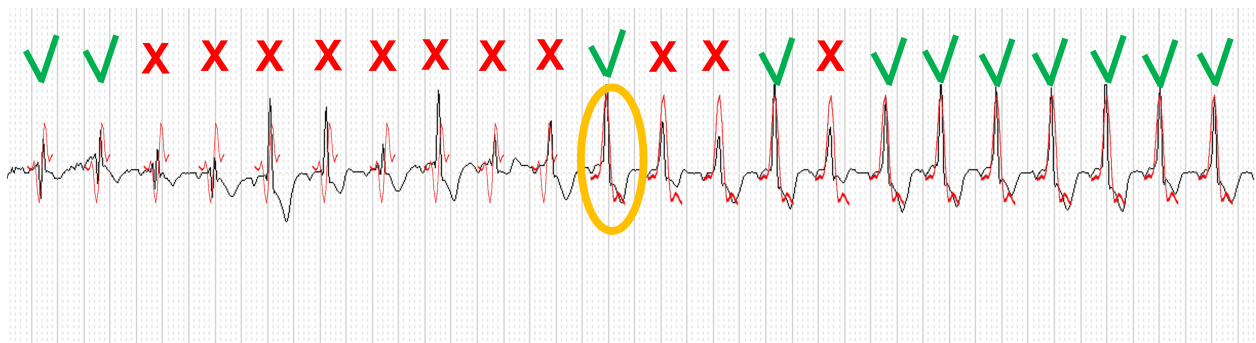
Figure 7.5: ECG example of QRS template update. The red crosses above the beats indicate no match between the template and the complexes, whereas the green checkmarks above the beats indicate a match.

premature ventricular contractions. The small beat in Figure 7.6a and the first red X in Figure 7.5 do not match the SR template, so they are counted as an abnormal heartbeat. The SR template is compared with each of the next 7 beats. Since these beats do not match the SR template, a VT template is generated, and the algorithm switches from the SR to the VT template for matching future beats. An example of a beat matching the VT template is shown in Figure 7.6b.

(a) SR template not matching a QRS complex

(b) VT template matching a QRS complex

Figure 7.6: Comparison between a template and a QRS complex before and after update

7.4   P Wave Detection

AF detection can be enhanced by the detection of P waves [8] [9] [99]. Since P wave shape can change over time, a P wave template is generated for each ECG segment. A typical P wave is depicted in Figure 2.1 and occurs in a P Wave Time Window defined from 300ms to 60ms before the R peak in a QRS complex. These R peaks are detected as described in Chapter 6. A P Wave Time Window must have a maximum signal value within a range consistent with P wave morphology to qualify as a candidate P wave. All candidate P waves in a segment are aligned and averaged as described in Section 7.2 to create a P wave template as shown in the example in Fig. 7.7. Candidate P waves that are similar to the P wave template using cross-correlation equation (7.2) are detected P waves.
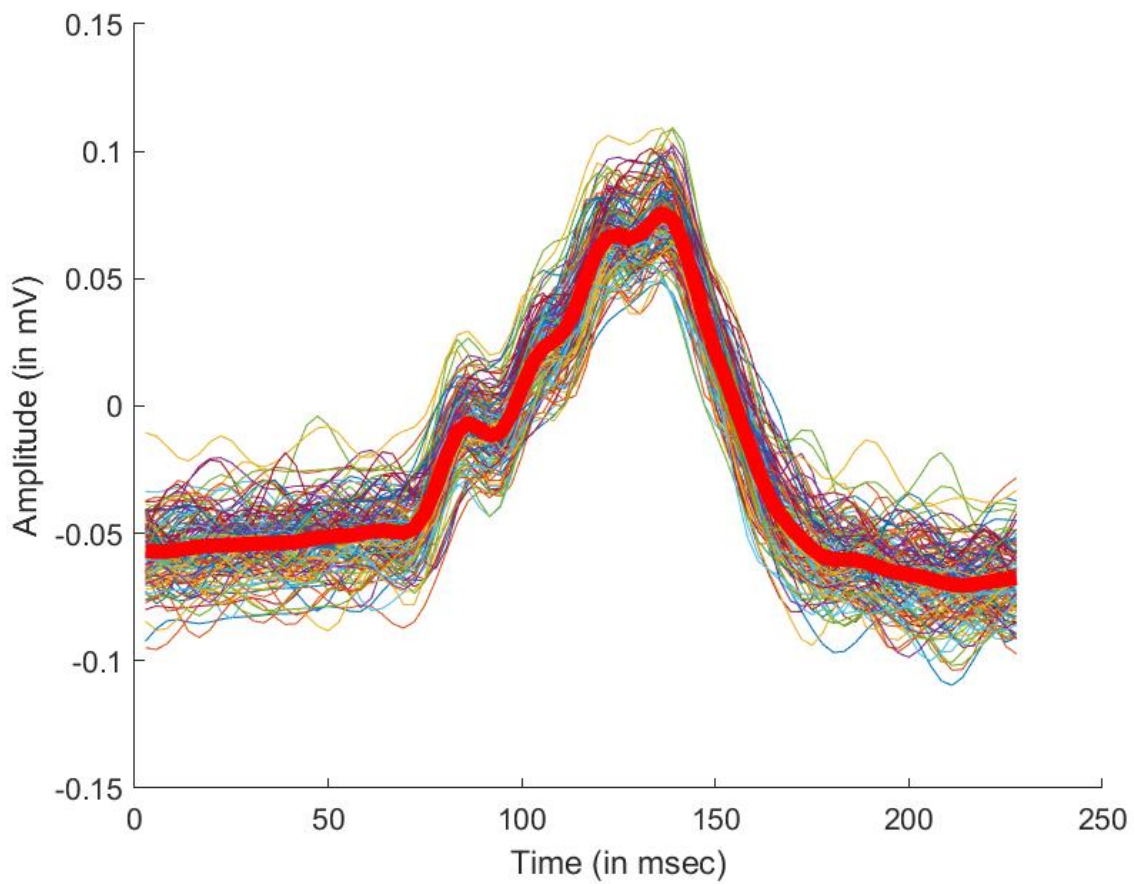
Figure 7.7: P wave template in red constructed by averaging candidate P waves in ECG segment

Chapter 8

Data Analysis

8.1 ECG Data

Data from the following four MIT-BIH databases are used to evaluate the AF detection algorithm: Arrhythmia Database [109], Atrial Fibrillation (AF) Database [110], Normal Sinus Rhythm (NSR) Database [111] [112], and Supraventricular Arrhythmia (SVA) Database [113]. The ECG signals were originally sampled at 360 Hz for Arrhythmia, 250 Hz for AF, and 128 Hz for NSR and SVA. For consistency, all signals were represented at a frequency of 360 Hz for analysis. The signals were divided into 2.5-minute segments where each segment is assigned a label of "AF" or "Not AF". The result is a total of 11,857 2.5-minute ECG segments from 167 patients. Table 8.1 shows the breakdown of ECG segments across the databases.

Table 8.1: Summary of MIT-BIH patient databases

Database	ECG Segments	Patients
Arrhythmia	1141	48
Atrial Fibrillation	581	23
Normal Sinus Rhythm	9200	18
Supraventricular Arrhythmia	935	78

8.2 Machine Learning

8.2.1 Descriptor Definition

Several descriptors that are derived from each ECG segment are used for AF detection. C is the RR consistency measure from equation (6.1) using Coefficient of Variation (CoV). C' is the RR consistency measure from equation (6.1) computed using only the detected QRS complexes in the segment that match the template using equation (7.3). N_R is the total number of detected R waves in the segment and $N_{R'}$ is the number of detected R waves in the segment that do not match the template. N_P is the number of P waves detected in the segment using the method in Section 7.4.

8.2.2 Model Generation

The data are split into training and testing sets with 5900 ECG segments in the training set and 5957 ECG segments in the testing set. The training data is used to build a model for the probability $P(\text{AF}|\, \overline{x})$ that a segment corresponds to AF given a vector of n explanatory variables $\overline{x} = (x_1, x_2, \ldots, x_n)$ that are derived from the features described in Section 8.2.1. The model is of the form

$$P(\text{AF}|\, \overline{x}) = \frac{1}{1 + e^{-S}} \tag{8.1}$$

where

$$S = c_0 + c_1 x_1 + c_2 x_2 + \cdots + c_n x_n \qquad (8.2)$$

and the c_i coefficients are derived from the training data using logistic regression [114]. The logistic function in equation (8.1) ensures that the probability $P(\text{AF}|\,\overline{x})$ will be between zero and one.

Three different models for $P(\text{AF}|\,\overline{x})$ are generated using different vectors $\overline{x}$ of explanatory variables. Model 1 considers only variables related to RR intervals. This is representative of current methods that are used in ICMs. Model 2 considers variables related to RR intervals and QRS template matching. Model 3 considers variables related to RR intervals, QRS template matching, and P wave detection. For each model, variables are included which have p-values that are less than 0.1. The estimated coefficients of the variables for each model and their standard errors and p-values are shown in Table 8.2 to Table 8.4.

Table 8.2: Table of estimated coefficients for model 1

Variable	Coefficient	SE	pValue
(Intercept)	-3.0551	0.0658	0.0000
C	0.0055	0.0016	0.0004

Table 8.3: Table of estimated coefficients for model 2

Variable	Coefficient	SE	pValue
(Intercept)	-0.6927	0.1129	0.0000
C	-0.0090	0.0034	0.0080
$N_{R'}$	-0.0871	0.0056	0.0000
$C * N_{R'}$	0.0004	0.0001	0.0081

Table 8.4: Table of estimated coefficients for model 3

Variable	Coefficient	SE	pValue
(Intercept)	-0.1978	0.1183	0.0945
C	-0.0077	0.0030	0.0111
$N_{R'}$	-0.0648	0.0050	0.0000
N_P	-0.3467	0.0029	0.0536
N_P/N_R	0.3489	0.1596	0.0289
$C' * N_P$	-0.0090	0.0016	0.0000

8.3   Results

A model $P(\mathrm{AF}|\ \bar{x})$ can be used to classify an ECG segment as "AF" or "Not AF" by computing the value of the model for the vector $\bar{x}$ for the segment and comparing to a threshold T. The three models described in Section 8.2.2 were used to define three algorithms for AF detection. Each algorithm was evaluated using the testing data. As we vary T for each algorithm, we obtain the receiver operating characteristic (ROC) curves shown in Figure 8.1. We see that performance improves as we add features from Algorithm 1 to Algorithm 2 to Algorithm 3. This shows the utility of using QRS template matching and P wave detection in addition to RR intervals. Table 8.5 shows the area under the ROC curve for each of the three algorithms.

Table 8.5: Tables of AUCs for AF detection

	Algorithm 1	Algorithm 2	Algorithm 3
Testing Set	0.8660	0.9393	0.9489
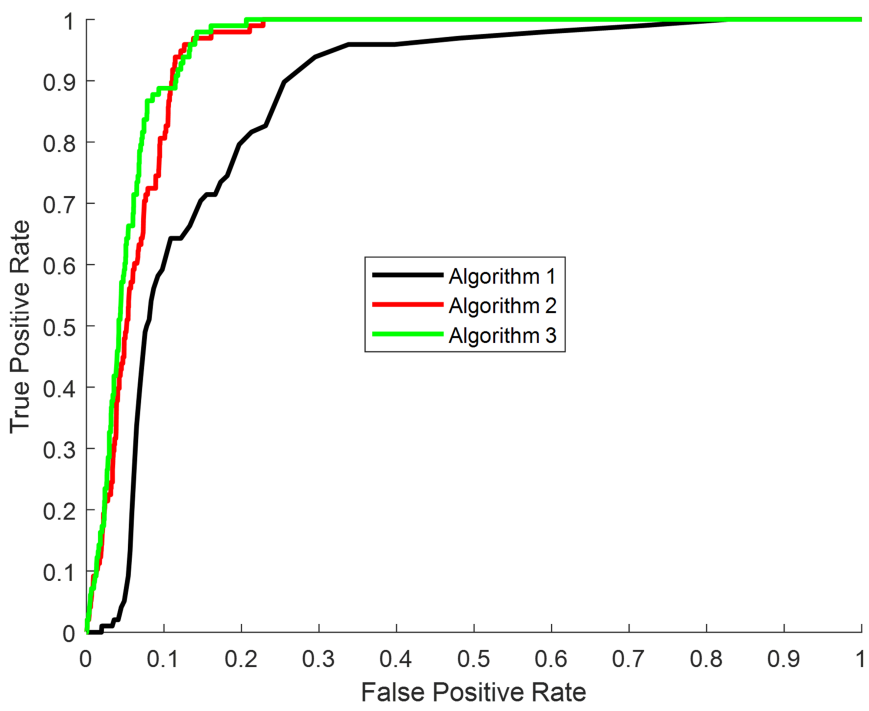
Figure 8.1: AFD ROC curves for three algorithms

Chapter 9

Conclusion

We have developed and demonstrated new methods for AF detection. The methods utilize adaptive templates for QRS complexes and P waves which allows use over long periods during which signal morphology can change. The algorithms are therefore amenable to use with devices such as insertable cardiac monitors that can continuously acquire ECGs for several months. We use a modular probabilistic methodology which enables detection performance to be quantified as we add ECG descriptors to the model. Data from four MIT-BIH databases are used to show that the approach is significantly more accurate than methods based on the consistency of RR intervals. We also show that the use of both QRS templates and P wave templates play an important role in AF detection.

Bibliography

[1] David Sanders, Leo Ungar, Michael A Eskander, and Arnold H Seto. Ambulatory ECG monitoring in the age of smartphones. *Clevel. Clin. J. Med*, 86:483–493, 2019.

[2] Rama Reddy Rajanna, Natarajan Sriraam, VS Prakash, Prabhu Ravikala Vittala, Uma Arun, and Sarthak Sahoo. External cardiac loop recorders: Functionalities, diagnostic efficacy, challenges and opportunities. volume 15, pages 273–292. IEEE, 2021.

[3] Mayo Clinic. Atrial fibrillation, 2017. `https://www.mayoclinic.org/diseases-conditions/atrial-fibrillation/symptoms-causes/syc-20350624` [Accessed June 11, 2022].

[4] Centers for Disease Control and Prevention. Atrial fibrillation, 2021. `https://www.cdc.gov/heartdisease/atrial_fibrillation.htm` [Accessed June 29, 2022].

[5] Centers for Disease Control and National Center for Health Statistics Prevention. About multiple cause of death, 1999–2019, 2019. `https://wonder.cdc.gov/controller/datarequest/D77` [Accessed June 29, 2022].

[6] Susan Colilla, Ann Crow, William Petkun, Daniel E Singer, Teresa Simon, and Xianchen Liu. Estimates of current and future incidence and prevalence of atrial fibrillation in the US adult population. *The American journal of cardiology*, 112(8):1142–1147, 2013.

[7] Yoko Miyasaka, Marion E Barnes, Bernard J Gersh, Stephen S Cha, Kent R Bailey, Walter P Abhayaratna, James B Seward, and Teresa SM Tsang. Secular trends in incidence of atrial fibrillation in Olmsted County, Minnesota, 1980 to 2000, and implications on the projections for future prevalence. *The American journal of cardiology*, 114(2):119–125, 2006.

[8] Abbott. Overview of Confirm Rx ICM with SharpSense Technology for Allied Health Professionals, 2020. `https://www.cardiovascular.abbott/us/en/hcp/products/cardiac-rhythm-management/insertable-cardiac-monitors/confirm-rx/procedure.html` [Accessed May 27, 2022].

[9] Helmut Pürerfellner, Prashanthan Sanders, Shantanu Sarkar, Erin Reisfeld, Jerry Reiland, Jodi Koehler, Evgeny Pokushalov, L'uboš Urban, and Lukas RC Dekker. Adapting detection sensitivity based on evidence of irregular sinus arrhythmia to improve

atrial fibrillation detection in insertable cardiac monitors. *EP Europace*, 20(FI_3):f321–f328, 2018.

[10] S Dash, KH Chon, S Lu, and EA Raeder. Automatic real time detection of atrial fibrillation. *Annals of biomedical engineering*, 37(9):1701–1709, 2009.

[11] Shantanu Sarkar, David Ritscher, and Rahul Mehra. A detector for a chronic implantable atrial tachyarrhythmia monitor. volume 55, pages 1219–1224. IEEE, 2008.

[12] Peng Zhang, Yuting Chen, Fan Lin, Sifan Wu, Xiaoyun Yang, and Qiang Li. Semi-supervised learning for automatic atrial fibrillation detection in 24-hour Holter monitoring. *IEEE Journal of Biomedical and Health Informatics*, 2022.

[13] Guadalupe García-Isla, Valentina Corino, and Luca Mainardi. Poincaré plot image and rhythm-specific atlas for atrial bigeminy and atrial fibrillation detection. *IEEE Journal of Biomedical and Health Informatics*, 25(4):1093–1100, 2020.

[14] Norbert Henzel, Janusz Wróbel, and Krzysztof Horoba. Atrial fibrillation episodes detection based on classification of heart rate derived features. In *2017 MIXDES-24th International Conference" Mixed Design of Integrated Circuits and Systems*, pages 571–576. IEEE, 2017.

[15] Vessela Krasteva and Irena Jekova. QRS template matching for recognition of ventricular ectopic beats. *Annals of biomedical engineering*, 35(12):2065–2076, 2007.

[16] Philip De Chazal. Detection of supraventricular and ventricular ectopic beats using a single lead ECG. In *2013 35th Annual International Conference of the IEEE Engineering in Medicine and Biology Society (EMBC)*, pages 45–48. IEEE, 2013.

[17] Arturo Martínez, Raúl Alcaraz, and José J Rieta. Ventricular activity morphological characterization: Ectopic beats removal in long term atrial fibrillation recordings. *Computer methods and programs in biomedicine*, 109(3):283–292, 2013.

[18] National Heart Lung and Blood Institute. How the heart works: The heart, 2022. `https://www.nhlbi.nih.gov/health/heartQ` [Accessed June 24, 2023].

[19] Medical News Today. Cardiovascular system: Function, organs, diseases, and more, 2021. `https://www.medicalnewstoday.com/articles/cardiovascular-system?utm_source=ReadNext#organs-and-tissues` [Accessed July 29, 2023].

[20] David A Elliott, Edwin P Kirk, Daniel Schaft, and Richard P Harvey. NK-2 class homeodomain proteins: conserved regulators of cardiogenesis. In *Heart development and regeneration*, pages 569–597. Elsevier, 2010.

[21] Center for Cardiac and Vascular Interventions. Heart arrhythmia, 2023. `https://cacvi.org/conditions/heart-conditions/heart-arrhythmia/` [Accessed July 29, 2023].

[22] National Heart Lung and Blood Institute. What are the signs and symptoms of an arrhythmia?, 2015. `http://www.nhlbi.nih.gov/health/health-topics/topics/arr/signs` [Accessed July 29, 2023].

[23] National Heart Lung and Blood Institute. What is arrhythmia?, 2015. `https://www.nhlbi.nih.gov/health/arrhythmias` [Accessed July 29, 2023].

[24] National Heart Lung and Blood Institute. Types of arrhythmia, 2015. `https://web.archive.org/web/20150607165144/http://www.nhlbi.nih.gov/health/health-topics/topics/arr/types` [Accessed July 29, 2023].

[25] Majid Haghjoo. Bradyarrhythmias. In *Practical Cardiology*, pages 289–296. Elsevier, 2022.

[26] NM Sokoloff. Bradyarrhythmias: AV conduction disturbances. *Geriatrics (Basel, Switzerland)*, 40(8):83–86, 1985.

[27] Mayo Clinic. Premature ventricular contraction, 2022. `https://www.mayoclinic.org/diseases-conditions/premature-ventricular-contractions/symptoms-causes/syc-20376757` [Accessed September 10, 2022].

[28] Medline Plus. Heart chambers, 2020. `https://medlineplus.gov/ency/imagepages/19612.htm` [Accessed September 5, 2022].

[29] Saira Aziz, Sajid Ahmed, and Mohamed-Slim Alouini. ECG-based machine-learning algorithms for heartbeat classification. *Scientific Reports*, 11(1):1–14, 2021.

[30] Mayo Clinic. Heart arrhythmia, 2023. `https://www.mayoclinic.org/diseases-conditions/heart-arrhythmia/symptoms-causes/syc-20350668` [Accessed July 29, 2023].

[31] Yuki Hagiwara, Hamido Fujita, Shu Lih Oh, Jen Hong Tan, Ru San Tan, Edward J Ciaccio, and U Rajendra Acharya. Computer-aided diagnosis of atrial fibrillation based on ECG signals: A review. *Information Sciences*, 467:99–114, 2018.

[32] U Rajendra Acharya, Hamido Fujita, Muhammad Adam, Oh Shu Lih, Tan Jen Hong, Vidya K Sudarshan, and Joel EW Koh. Automated characterization of arrhythmias using nonlinear features from tachycardia ECG beats. In *2016 IEEE international conference on systems, man, and cybernetics (SMC)*, pages 000533–000538. IEEE, 2016.

[33] Mayo Clinic. Atrial flutter, 2022. `https://www.mayoclinic.org/diseases-conditions/atrial-flutter/symptoms-causes/syc-20352586` [Accessed June 25, 2023].

[34] Mayo Clinic. Supraventricular Tachycardia - Atrioventricular nodal reentry tachycardia (AVNRT), 2022. `https://www.mayoclinic.org/diseases-conditions/avnrt/cdc-20355254` [Accessed September 10, 2022].

[35] Mayo Clinic. Ventricular tachycardia, 2022. `https://www.mayoclinic.org/diseases-conditions/ventricular-tachycardia/symptoms-causes/syc-20355138` [Accessed September 10, 2022].

[36] Mayo Clinic. Ventricular fibrillation, 2021. `https://www.mayoclinic.org/diseases-conditions/ventricular-fibrillation/symptoms-causes/syc-20364523` [Accessed September 10, 2022].

[37] Mayo Clinic. Sick sinus syndrome, 2022. `https://www.mayoclinic.org/diseases-conditions/sick-sinus-syndrome/symptoms-causes/syc-20377554` [Accessed June 26, 2022].

[38] National Center for Biotechnology Information. Sick sinus syndrome, 2023. `https://www.ncbi.nlm.nih.gov/books/NBK470599/` [Accessed June 26, 2023].

[39] National Center for Biotechnology Information. First-degree heart block, 2023. `https://www.ncbi.nlm.nih.gov/books/NBK448164/` [Accessed July 17, 2023].

[40] National Center for Biotechnology Information. Second-degree heart block, 2022. `https://www.ncbi.nlm.nih.gov/books/NBK482359/` [Accessed July 17, 2023].

[41] National Center for Biotechnology Information. Third-degree heart block, 2023. `https://www.ncbi.nlm.nih.gov/books/NBK545199/` [Accessed July 17, 2023].

[42] Euijae Lee, Eue-Keun Choi, Kyung-Do Han, HyunJung Lee, Won-Seok Choe, So-Ryoung Lee, Myung-Jin Cha, Woo-Hyun Lim, Yong-Jin Kim, and Seil Oh. Mortality and causes of death in patients with atrial fibrillation: a nationwide population-based study. *PLoS One*, 13(12):209687, 2021.

[43] Adel Khalifa Sultan Hamad. New technologies for detection and management of atrial fibrillation. *Journal of the Saudi Heart Association*, 33(2):169, 2021.

[44] Oliver Faust, Edward J Ciaccio, and U Rajendra Acharya. A review of atrial fibrillation detection methods as a service. *International journal of environmental research and public health*, 17(9):3093, 2020.

[45] Hyun Jun Cho, Cheol Hyun Lee, Jongmin Hwang, Hyoung-Seob Park, Sang-Woong Choi, In-Cheol Kim, Yun-Kyeong Cho, Hyuck-Jun Yoon, Hyungseop Kim, Chang-Wook Nam, et al. Accuracy of implantable loop recorders for detecting atrial tachyarrhythmias after atrial fibrillation catheter ablation. *International Journal of Arrhythmia*, 21:1–7, 2020.

[46] Fatma Murat, Ferhat Sadak, Ozal Yildirim, Muhammed Talo, Ender Murat, Murat Karabatak, Yakup Demir, Ru-San Tan, and U Rajendra Acharya. Review of deep learning-based atrial fibrillation detection studies. *International journal of environmental research and public health*, 18(21):11302, 2021.

[47] Jo Woon Chong, Chae Ho Cho, Fatemehsadat Tabei, Duy Nada Le-Anh, Esa, David D. McManus, and Ki H. Chon. Motion and noise artifact-resilient atrial fibrillation detection using a smartphone. *IEEE journal on emerging and selected topics in circuits and systems*, 8(2):230–239, 2018.

[48] Stephanie C Sun, Xiaoyi Min, and Glenn Healey. Investigation of Key Variables Impacting ICM Sensing Using Computer Simulations. In *2018 40th Annual International Conference of the IEEE Engineering in Medicine and Biology Society (EMBC)*, pages 1156–1160. IEEE, 2018.

[49] Tom Fawcett. An introduction to ROC analysis. *Pattern recognition letters*, 27(8):861–874, 2006.

[50] Jinho Park, Sangwook Lee, and Moongu Jeon. Atrial fibrillation detection by heart rate variability in Poincare plot. *Biomedical engineering online*, 8(1):1–12, 2009.

[51] K Tateno and L Glass. A method for detection of atrial fibrillation using RR intervals. *Computers in Cardiology 2000*, 27:391–394, 2000.

[52] K Tateno and L Glass. Automatic detection of atrial fibrillation using the coefficient of variation and density histograms of RR and ΔRR intervals. *Medical and Biological Engineering and Computing*, 39(6):664–671, 2001.

[53] Georg Noelker, Julia Mayer, Leif-Hendrik Boldt, Karlheinz Seidl, Vincent Van Driel, Thomas Massa, Marc Kollum, Johannes Brachmann, Thomas Deneke, Gerhard Hindricks, Werner Jung, Kyle J Brunner, Stacia Kraus, Alexander Hummer, and Thorsten Lewalter. Performance of an implantable cardiac monitor to detect atrial fibrillation: results of the DETECT AF study. *Journal of Cardiovascular Electrophysiology*, 27(12):1403–1410, 2016.

[54] Jiapu Pan and Willis J Tompkins. A Real-Time QRS Detection Algorithm. volume 3, pages 230–236, 1985.

[55] Pavan D Paikrao, Deeplaxmi P Shinde, and VV Ingale. Peak detection algorithm for ECG wave. In *2011 International Conference on Emerging Trends in Networks and Computer Communications (ETNCC)*, pages 421–423. IEEE, 2011.

[56] Suneet Mittal, John Rogers, Shantanu Sarkar, Jodi Koehler, Eduardo N Warman, Todd T Tomson, and Rod S Passman. Real-world performance of an enhanced atrial fibrillation detection algorithm in an insertable cardiac monitor. *Heart Rhythm*, 13(8):1624–1630, 2016.

[57] Gergely Tuboly, György Kozmann, Orsolya Kiss, and Béla Merkely. Atrial Fibrillation Detection Based on Poincaré Plot and P Wave Analysis. *In 2019 12th International Conference on Measurement*, pages 17–20, 2019.

[58] Sidrah Liaqat, Kia Dashtipour, Adnan Zahid, Kamran Arshad, Sana Ullah Jan, Khaled Assaleh, and Naeem Ramzan. A review and comparison of the state-of-the-art techniques for atrial fibrillation detection and skin hydration. *Frontiers in Communications and Networks*, 2:679502, 2021.

[59] Sujit Kumar Sahoo, Wenmiao Lu, Sintiani Dewi Teddy, Desok Kim, and Mengling Feng. Detection of atrial fibrillation from non-episodic ECG data: a review of methods. In *2011 Annual International Conference of the IEEE Engineering in Medicine and Biology Society*, pages 4992–4995. IEEE, 2011.

[60] Justin G Yoon, Munes Fares, Walter Hoyt, and Christopher S Snyder. Diagnostic accuracy and safety of Confirm Rx^{TM} insertable cardiac monitor in pediatric patients. *Pediatric Cardiology*, 42:142–147, 2021.

[61] Joseph Rossano, Beatrijs Bloemers, Narayanswami Sreeram, Seshadri Balaji, and Maully J Shah. Efficacy of implantable loop recorders in establishing symptom-rhythm correlation in young patients with syncope and palpitations. *Pediatrics*, 112(3):e228–e233, 2003.

[62] Antonio Bisignani, Silvana De Bonis, Luigi Mancuso, Gianluca Ceravolo, and Giovanni Bisignani. Implantable loop recorder in clinical practice. *Journal of arrhythmia*, 35(1):25–32, 2019.

[63] Shaun Giancaterino, Florentino Lupercio, Marin Nishimura, and Jonathan C Hsu. Current and future use of insertable cardiac monitors. *JACC: Clinical Electrophysiology*, 4(11):1383–1396, 2018.

[64] Deepak Padmanabhan, Krishna Kancharla, Majd A El-Harasis, Ameesh Isath, Nayani Makkar, Peter A Noseworthy, Paul A Friedman, Yong-Mei Cha, and Suraj Kapa. Diagnostic and therapeutic value of implantable loop recorder: A tertiary care center experience. *Pacing and Clinical Electrophysiology*, 42(1):38–45, 2019.

[65] Aeshita Dwivedi, Jacqueline Joza, Kabir Malkani, Todd B Mendelson, Silvia G Priori, Larry A Chinitz, Steven J Fowler, and Marina Cerrone. Implantable loop recorder in inherited arrhythmia diseases: a critical tool for symptom diagnosis and advanced risk stratification. *JACC: Clinical Electrophysiology*, 4(10):1372–1374, 2018.

[66] Giuseppe Ciconte, Massimo Saviano, Luigi Giannelli, Zarko Calovic, Mario Baldi, Cristiano Ciaccio, Amarild Cuko, Raffaele Vitale, Daniele Giacopelli, Manuel Conti, Felicia Lipartiti, Federica Giordano, Fabio Maresca, Mario Moscatiello, Gabriele Vicedomini, Vincenzo Santinelli, and Carlo Pappone. Atrial fibrillation detection using a novel three-vector cardiac implantable monitor: the atrial fibrillation detect study. *Ep Europace*, 19(7):1101–1108, 2017.

[67] Rafi Sakhi, Dominic AMJ Theuns, Tamas Szili-Torok, and Sing-Chien Yap. Insertable cardiac monitors: current indications and devices. *Expert review of medical devices*, 16(1):45–55, 2019.

[68] Christopher M Bishop and Nasser M Nasrabadi. *Pattern recognition and machine learning*, volume 4. Springer, 2006.

[69] Jinseok Lee, Yunyoung Nam, David D McManus, and Ki H Chon. Time-varying coherence function for atrial fibrillation detection. *IEEE Transactions on Biomedical Engineering*, 60(10):2783–2793, 2013.

[70] Alex Graves, Abdel-rahman Mohamed, and Geoffrey Hinton. Speech recognition with deep recurrent neural networks. In *2013 IEEE international conference on acoustics, speech and signal processing*, pages 6645–6649. IEEE, 2013.

[71] Arik Poznanski and Lior Wolf. CNN-N-Gram for handwriting word recognition. In *Proceedings of the IEEE conference on computer vision and pattern recognition*, pages 2305–2314, 2016.

[72] Alex Krizhevsky, Ilya Sutskever, and Geoffrey E Hinton. Imagenet classification with deep convolutional neural networks. *Advances in neural information processing systems*, 25, 2012.

[73] June-Goo Lee, Sanghoon Jun, Young-Won Cho, Hyunna Lee, Guk Bae Kim, Joon Beom Seo, and Namkug Kim. Deep learning in medical imaging: general overview. *Korean journal of radiology*, 18(4):570–584, 2017.

[74] U Rajendra Acharya, Hamido Fujita, Oh Shu Lih, Muhammad Adam, Jen Hong Tan, and Chua Kuang Chua. Automated detection of coronary artery disease using different durations of ECG segments with convolutional neural network. *Knowledge-Based Systems*, 132:62–71, 2017.

[75] U Rajendra Acharya, Hamido Fujita, Oh Shu Lih, Yuki Hagiwara, Jen Hong Tan, and Muhammad Adam. Automated detection of arrhythmias using different intervals of tachycardia ECG segments with convolutional neural network. *Information sciences*, 405:81–90, 2017.

[76] U Rajendra Acharya, Hamido Fujita, Shu Lih Oh, Yuki Hagiwara, Jen Hong Tan, and Muhammad Adam. Application of deep convolutional neural network for automated detection of myocardial infarction using ECG signals. *Information Sciences*, 415:190–198, 2017.

[77] U Rajendra Acharya, Hamido Fujita, Shu Lih Oh, U Raghavendra, Jen Hong Tan, Muhammad Adam, Arkadiusz Gertych, and Yuki Hagiwara. Automated identification of shockable and non-shockable life-threatening ventricular arrhythmias using convolutional neural network. *Future Generation Computer Systems*, 79:952–959, 2018.

[78] U Rajendra Acharya, Shu Lih Oh, Yuki Hagiwara, Jen Hong Tan, Muhammad Adam, Arkadiusz Gertych, and Ru San Tan. A deep convolutional neural network model to classify heartbeats. *Computers in biology and medicine*, 89:389–396, 2017.

[79] Jen Hong Tan, Yuki Hagiwara, Winnie Pang, Ivy Lim, Shu Lih Oh, Muhammad Adam, Ru San Tan, Ming Chen, and U Rajendra Acharya. Application of stacked convolutional and long short-term memory network for accurate identification of CAD ECG signals. *Computers in biology and medicine*, 94:19–26, 2018.

[80] Zhenjie Yao, Zhiyong Zhu, and Yixin Chen. Atrial fibrillation detection by multi-scale convolutional neural networks. In *2017 20th international conference on information fusion (Fusion)*, pages 1–6. IEEE, 2017.

[81] Chan Yuan, Yan Yan, Lin Zhou, Jingwen Bai, and Lei Wang. Automated atrial fibrillation detection based on deep learning network. In *2016 IEEE International Conference on Information and Automation (ICIA)*, pages 1159–1164. IEEE, 2016.

[82] Lu Liu, Syed Aziz Shah, Guoqing Zhao, and Xiaodong Yang. Respiration symptoms monitoring in body area networks. *Applied Sciences*, 8(4):568, 2018.

[83] Kia Dashtipour, Mandar Gogate, Jingpeng Li, Fengling Jiang, Bin Kong, and Amir Hussain. A hybrid Persian sentiment analysis framework: Integrating dependency grammar based rules and deep neural networks. *Neurocomputing*, 380:1–10, 2020.

[84] William Taylor, Syed Aziz Shah, Kia Dashtipour, Adnan Zahid, Qammer H Abbasi, and Muhammad Ali Imran. An intelligent non-invasive real-time human activity recognition system for next-generation healthcare. *Sensors*, 20(9):2653, 2020.

[85] Fengling Jiang, Bin Kong, Jingpeng Li, Kia Dashtipour, and Mandar Gogate. Robust visual saliency optimization based on bidirectional Markov chains. *Cognitive Computation*, 13:69–80, 2021.

[86] Kia Dashtipour, Mandar Gogate, Ahsan Adeel, Amir Hussain, Abdulrahman Alqarafi, and Tariq Durrani. A comparative study of Persian sentiment analysis based on different feature combinations. In *Communications, Signal Processing, and Systems: Proceedings of the 2017 International Conference on Communications, Signal Processing, and Systems*, pages 2288–2294. Springer, 2019.

[87] Sana Ullah Jan, Young-Doo Lee, Jungpil Shin, and Insoo Koo. Sensor fault classification based on support vector machine and statistical time-domain features. *IEEE Access*, 5:8682–8690, 2017.

[88] Sana Ullah Jan and Insoo Koo. A novel feature selection scheme and a diversified-input SVM-based classifier for sensor fault classification. *Journal of Sensors*, 2018, 2018.

[89] Syed Muhammad Asad, Kia Dashtipour, Sajjad Hussain, Qammer Hussain Abbasi, and Muhammad Ali Imran. Travelers-tracing and mobility profiling using machine learning in railway systems. In *2020 International Conference on UK-China Emerging Technologies (UCET)*, pages 1–4. IEEE, 2020.

[90] Mark Lown, Michael Brown, Chloë Brown, Arthur M Yue, Benoy N Shah, Simon J Corbett, George Lewith, Beth Stuart, Michael Moore, and Paul Little. Machine learning detection of atrial fibrillation using wearable technology. *PloS one*, 15(1):e0227401, 2020.

[91] Mandar Gogate, Amir Hussain, and Kaizhu Huang. Random features and random neurons for brain-inspired big data analytics. In *2019 international conference on data mining workshops (ICDMW)*, pages 522–529. IEEE, 2019.

[92] Xiaoyan Xu, Shoushui Wei, Caiyun Ma, Kan Luo, Li Zhang, and Chengyu Liu. Atrial fibrillation beat identification using the combination of modified frequency slice wavelet transform and convolutional neural networks. *Journal of healthcare engineering*, 2018, 2018.

[93] Jonathan Mant, FD Richard Hobbs, Kate Fletcher, Andrea Roalfe, David Fitzmaurice, Gregory YH Lip, and Ellen Murray. Warfarin versus aspirin for stroke prevention in an elderly community population with atrial fibrillation (the Birmingham Atrial Fibrillation Treatment of the Aged Study, BAFTA): a randomised controlled trial. *The Lancet*, 370(9586):493–503, 2007.

[94] Nicole Lowres, Lis Neubeck, Glenn Salkeld, Ines Krass, Andrew J McLachlan, Julie Redfern, Alexandra A Bennett, Tom Briffa, Adrian Bauman, Carlos Martinez, et al. Feasibility and cost-effectiveness of stroke prevention through community screening for atrial fibrillation using iPhone ECG in pharmacies. *Thrombosis and haemostasis*, 111(06):1167–1176, 2014.

[95] Georga Cooke, Jenny Doust, and Sharon Sanders. Is pulse palpation helpful in detecting atrial fibrillation? a systematic review: particular high-risk patients may benefit from repeated testing. *Journal of family practice*, 55(2):130–135, 2006.

[96] Rod S Passman, John D Rogers, Shantanu Sarkar, Jerry Reiland, Erin Reisfeld, Jodi Koehler, and Suneet Mittal. Development and validation of a dual sensing scheme to improve accuracy of bradycardia and pause detection in an insertable cardiac monitor. *Heart Rhythm*, 14(7):1016–1023, 2017.

[97] Philipp Lacour, Phi Long Dang, Martin Huemer, Abdul Shokor Parwani, Philipp Attanasio, Burkert Pieske, Leif-Hendrik BOLDT, Wilhelm Haverkamp, and Florian Blaschke. Performance of the new BioMonitor 2-AF insertable cardiac monitoring system: Can better be worse? *Pacing and Clinical Electrophysiology*, 40(5):516–526, 2017.

[98] G. Kushner et al. Relationship of body mass index to ventricular sensing with the LINQ implantable loop recorder. *Heart Rhythm*, pages 6–30, 2015.

[99] Helmut Pürerfellner, Evgeny Pokushalov, Shantanu Sarkar, Jodi Koehler, Ren Zhou, Lubos Urban, and Gerhard Hindricks. P-wave evidence as a method for improving algorithm to detect atrial fibrillation in insertable cardiac monitors. *Heart Rhythm*, 11(9):1575–1583, 2014.

[100] Prashanthan Sanders, Helmut Pürerfellner, Evgeny Pokushalov, Shantanu Sarkar, Marco Di Bacco, Bärbel Maus, Lukas RC Dekker, et al. Performance of a new atrial fibrillation detection algorithm in a miniaturized insertable cardiac monitor: Results from the Reveal LINQ Usability Study. *Heart Rhythm*, 13(7):1425–1430, 2016.

[101] ZMT Zurich MedTech AG. Sim4Life, 2010. `https://www.zurichmedtech.com/sim4life/` [Accessed June 24, 2016].

[102] PA Hasgall, F Di Gennaro, C Baumgartner, E Neufeld, MC Gosselin, D Payne, A Klingenböck, and N Kuster. Itis database for thermal and electromagnetic parameters of biological tissues, version 3.0, 2015.

[103] IT'IS Foundation. Virtual population tissue properties, 2010. `https://www.itis.ethz.ch/virtual-population/tissue-properties/overview/` [Accessed June 25, 2017].

[104] A. Minchole and E. Zacur. Snapshot of the simulated cardiac electrical activity, 2016. `http://www.archer.ac.uk/about-archer/news-events/events/image-comp/gallery-2016/` [Accessed July 7, 2017].

[105] A. Minchole and E. Zacur. Snapshot of the simulated cardiac electrical activity for a personalized model from a 65 years old man MRI, 2016. `http://www.archer.ac.uk/about-archer/news-events/events/image-comp/gallery-2016/` [Accessed July 7, 2017].

[106] Bruno Taccardi, Luigi De Ambroggi, and Domenico Riva. Chest maps of heart potentials in right bundle branch block. *Journal of Electrocardiology*, 2(2):109–116, 1969.

[107] Signe S Risom, Marianne W Nørgaard, and Megan M Streur. Quality of life and symptom experience measurement tools in adults with atrial fibrillation: a scoping review protocol. *JBI evidence synthesis*, 20(5):1376–1384, 2022.

[108] Desok Kim, Yunhwan Seo, Woo Ram Jung, and Chan-Hyun Youn. Detection of long term variations of heart rate variability in normal sinus rhythm and atrial fibrillation ECG data. In *2008 International Conference on BioMedical Engineering and Informatics*, volume 2, pages 404–408. IEEE, 2008.

[109] George B Moody and Roger G Mark. The impact of the MIT-BIH arrhythmia database. *IEEE Engineering in Medicine and Biology Magazine*, 20(3):45–50, 2001.

[110] George Moody. A new method for detecting atrial fibrillation using RR intervals. *Computers in Cardiology*, pages 227–230, 1983.

[111] GB Moody, WE Muldrow, and RG Mark. MIT-BIH normal sinus rhythm database. *PhysioNet. doi*, 10:C2NK5R, 1999.

[112] Ary L Goldberger, Luis AN Amaral, Leon Glass, Jeffrey M Hausdorff, Plamen Ch Ivanov, Roger G Mark, Joseph E Mietus, George B Moody, Chung-Kang Peng, and H Eugene Stanley. PhysioBank, PhysioToolkit, and PhysioNet: components of a new research resource for complex physiologic signals. *Circulation*, 101(23):e215–e220, 2000.

[113] Scott David Greenwald, Ramesh S Patil, and Roger G Mark. Improved detection and classification of arrhythmias in noise-corrupted electrocardiograms using contextual information. In *Proceedings Computers in Cardiology*, pages 461–464. IEEE, 1990.

[114] DW Hosmer and S Lemeshow. *Applied Logistic Regression*. Wiley, 2000.